
Chapter 23

Bistatic Radar

Nicholas J. Willis

Technology Service Corporation (retired)

23.1 CONCEPT AND DEFINITIONS

A bistatic radar uses antennas at separate sites for transmission and reception. The transmitter and receiver can be, and usually are, located at those sites to minimize transmission line losses. In nearly all cases of bistatic operation, antenna separation is selected to achieve some operational, technical, or cost benefit, and is usually a significant fraction of the target range.¹ Bistatic radars have been designed, developed, tested, and in some cases, deployed for military, commercial, and scientific applications. Typical military applications include air and space surveillance and range instrumentation. Commercial applications include wind field measurements and traffic surveillance. Scientific applications include measurement of planetary surfaces and atmospheres and study of ionospheric turbulence. Examples are given in Section 23.4. While these examples are both credible and useful, they are niche applications when compared to the ubiquitous capabilities of monostatic radars, which remain the principal method for *radio detection and ranging*.

Bistatic radars can operate with *dedicated transmitters*, which are designed for bistatic operation and controlled by the bistatic radar, or with *transmitters-of-opportunity*, which are designed for other purposes but found suitable for bistatic operation even when not controlled by the bistatic radar. When the transmitter of opportunity is from a monostatic radar, the bistatic radar is often called a *hitchhiker*. When the transmitter of opportunity is from a broadcast station or communications link, sources other than a radar, the bistatic radar has been called many things including *passive radar*, *passive bistatic radar*, *passive coherent location*, *parasitic radar*, and *piggy-back radar*.² Transmitters-of-opportunity in military scenarios can be designated either *cooperative* or *noncooperative*, where cooperative denotes an allied or friendly transmitter and noncooperative denotes a hostile or neutral transmitter.

Bistatic target detection uses a process similar to that of a monostatic radar, where the target is illuminated by a transmitter and target echoes are received, detected, and processed by a receiver. When operating with transmitters using CW or high-duty cycle waveforms, a bistatic receiver may need to augment its spatial isolation with spatial and/or spectral cancellation to reduce the transmitter's *direct-path* feed-through to acceptable levels. The bistatic radar can also use a portion of the residual or uncancelled direct-path transmit signal as a reference in a *correlation receiver*, which cross-correlates the received and transmitted signals, emulating matched filter operation.

Bistatic target location uses a process different from that of a monostatic radar. In a typical implementation, the bistatic radar measures (a) the transmitter-to-target-to-receiver propagation time, converted to a transmitter-to-target plus target-to-receiver *range-sum*; (b) the target direction-of-arrival (DOA) from the receiver; and (c) the transmitter-to-receiver distance, or *baseline*, to solve the transmitter-target-receiver triangle, called the *bistatic triangle*. This triangle locates the target, usually in terms of a range and angle referenced to the receive site. Other location schemes are given in Section 23.6.

When separate transmit and receive antennas are at a single site, as is common in CW radars, the radar has characteristics of a monostatic radar, and the term *bistatic* is not used to describe such a system. In special cases, the antennas can be at separate sites, and the radar is still considered to operate monostatically. For example, an over-the-horizon (OTH) radar can have a site separation of 100 km or more to achieve adequate transmit signal isolation. But that separation is small compared to the target range of thousands of kilometers, and the radar again operates with monostatic characteristics.

A variation of the bistatic radar is the *multistatic radar*, which uses multiple antennas at separate locations, one antenna for transmission and multiple antennas—each at a different location—for reception, or vice versa. Again, transmitters or receivers are usually sited with the antennas. Target detection is done bistatically, with each transmit-receive pair performing independent detections within a surveillance region common to all such pairs. Target location typically measures the baseline and takes simultaneous range-sum measurements from multiple transmitter-receiver pairs, which are plotted as ellipses with a transmitter-receiver pair at each ellipse foci. The intersection of these ellipses, or *constant range-sum contours*, locate the target. It is similar to *multilateration* because only range measurements are used to locate the target.*

A multistatic radar can also use *triangulation* for target location by taking simultaneous target DOA measurements from multiple receive sites at known locations. It is used by *SPASUR*¹² as a brute-force, satellite location technique. However, because of the large aperture sizes (or array lengths) required for sufficiently accurate DOA measurements at useful ranges, triangulation is seldom considered for other applications.

Concepts, data, and expressions developed for bistatic radars often apply to multistatic radars, for example, the range equation, target doppler, target radar cross section, and surface clutter. Thus, the remainder of this chapter will concentrate on the bistatic radar topic, developing multistatic excursions and deviations only when necessary.

Passive receiving systems, or *electronic support measure (ESM)* systems, often use two or more receiving sites. Their purpose is typically to detect, identify, and locate transmitters such as those from monostatic radars. They are also called *emitter locators*. Target location is by means of combined angle measurements from each site (e.g., triangulation) or time-difference-of-arrival and/or differential doppler measurements between sites (e.g., multilateration). These systems usually are not designed to detect and process the echoes from targets illuminated by the transmitter. They can, however, be used by a bistatic hitchhiker to identify and locate a suitable transmitter. Thus, although they have many requirements and characteristics common to multistatic radars, they are not radars and will not be considered here.

* The foregoing describes multistatic operation that combines data noncoherently. Coherent data combining is also possible where for example in-phase and quadrature data from each receive site is combined to form a large receive aperture. Examples include thinned, random, distorted, and distributed arrays,³⁻⁷ interferometric radars,^{8,9} and the radio camera.^{10,11} This subject is treated further in Willis.¹

The foregoing definitions are broad and traditional^{13–16} but are by no means uniformly established in the literature. Terms such as *quasi-bistatic*, *quasi-monostatic*, *pseudo-monostatic*, *tristatic*, *polystatic*, *real multistatic*, *multi-bistatic*, and *netted bistatic* have also been used.^{17–20} They are usually special cases of the broad definitions given above. The term *pseudo-monostatic* will be used to characterize bistatic geometries that approximate monostatic operation.

23.2 COORDINATE SYSTEMS

A two-dimensional north-referenced coordinate system²¹ is used throughout this chapter. Figure 23.1 shows the coordinate system and parameters defining bistatic radar operation in the (x, y) plane, also called the *bistatic plane*.²² The bistatic triangle lies in the bistatic plane. The distance L between the transmitter and the receiver is called the *baseline range* or simply the *baseline*; R_T is the range between transmitter and target; and R_R is the range between receiver and target. The angles θ_T and θ_R are, respectively, the transmitter and receiver *look angles*, which are taken as positive when measured clockwise from north. They are also called direction-of-arrival (DOA), angle-of-arrival (AOA), or line-of-sight (LOS). The *bistatic angle*, $\beta = \theta_T - \theta_R$, is the angle between the transmitter and receiver with the vertex at the target. It is also called the *cut angle* or the *scattering angle*. It is convenient to use β in calculations of target-related parameters and θ_T and θ_R in calculations of transmitter- and receiver-related parameters.

The transmitter-to-target-to-receiver range measured by a bistatic radar is the range sum ($R_T + R_R$). Methods for measuring this sum are given in Section 23.6. The range sum locates the target somewhere on the surface of an ellipsoid whose foci are the transmitter and receiver sites. The intersection of the bistatic plane and this ellipsoid

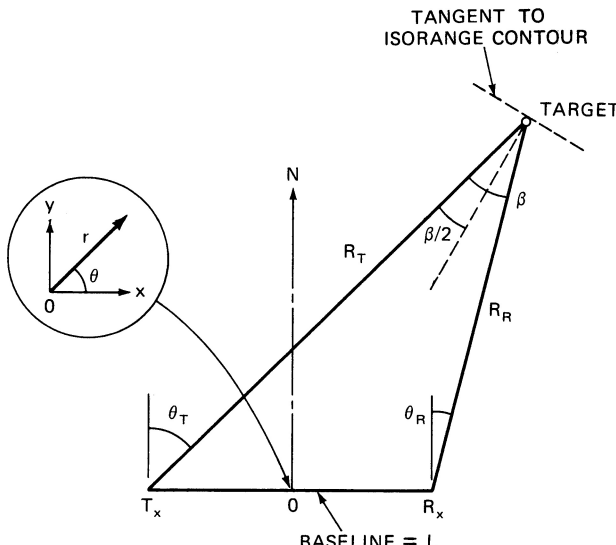


FIGURE 23.1 Bistatic radar north coordinate system for two dimensions, establishing the bistatic plane. The bistatic triangle lies in the bistatic plane.

produces the familiar ellipses of constant range sum, or *isorange contours*. A useful relationship is that the bisector of the bistatic angle is orthogonal to the tangent of that ellipse at the target. The tangent is often a good approximation to an isorange contour within the area common to the transmit and receive beams.

When the bistatic radar's receiving antenna is a phased array, and the array normal is also normal to the baseline, θ_R is measured directly by the antenna in any bistatic plane. This fortuitous situation is caused by *conic distortion*, which is inherent in any phased array antenna. However, when the array normal is not normal to the baseline, or when the receiving antenna is mechanically steered or scanned, θ_R is not measured directly. Often DOA measurements are taken in—or converted to—azimuth and elevation angles referenced to an x - y - z coordinate system centered at the receive site, where z is co-linear with the local vertical. Conversion between a north coordinate system and an x - y - z coordinate system is given in Section 5.3 of Willis.¹

Other coordinate systems, including three-dimensional systems, have been used to define bistatic radar operation.^{14,23–29} A polar coordinate system is also shown in Figure 23.1. The (r, θ) coordinates are located on the bistatic plane with origin at the midpoint of the baseline. It is useful for plotting *ovals of Cassini* (see Section 23.3) and is detailed in Willis.¹ On occasion, the included angles θ_T' and θ_R' are used to define transmitter and receiver look angles in the bistatic triangle, such that $\theta_T' + \theta_R' + \beta = 180^\circ$. In this case, $\theta_T' = 90^\circ - \theta_T$ and $\theta_R' = 90^\circ + \theta_R$ can be used to transform north-referenced equations into included-angle equations. Plots of bistatic clutter data use a separate and quite arcane coordinate system, which is defined in Section 23.8.

Geometry is a principal factor distinguishing bistatic from monostatic radar operation. In evaluating bistatic radar operation, it is useful to start with a geometry-invariant performance measure, which is obtained by setting $L = 0$ (or $R_T = R_R$ and $\beta = 0^\circ$). The result is defined as an *equivalent monostatic range*, or *benchmark range*, and is detailed in Section 23.3. It is also useful as a *sanity check*; because at these limits, all bistatic radar equations must reduce to an equivalent monostatic equation.

23.3 BISTATIC RADAR EQUATION

Benchmark Range Concept. Unlike a monostatic radar, the range performance of a bistatic radar is a function of the geometry, specifically the baseline range L and an antenna look angle, either θ_T or θ_R . When factors such as diffraction, refraction, multipath, and masking are absent or can be ignored, bistatic range as a function of these variables can be plotted on the bistatic plane using an oval of Cassini. An oval of Cassini is the locus of the vertex of a triangle when the product of the sides adjacent to the vertex is constant and the length of the opposite side is fixed. When applied to the bistatic triangle shown in Figure 23.1, the vertex is at the target; R_T and R_R are the sides adjacent to the vertex; and the baseline L is the length of the fixed, opposite side.

Traditionally, ovals of Cassini are drawn as contours of a constant received signal power or a received signal-to-noise ratio around a fixed baseline range, L . Although these signal-dependent contours provide a sense of bistatic radar performance, they do not show maximum/minimum detection ranges and coverage for variable baselines, all parameters of operational interest. To remedy this problem, the concept of a bistatic *benchmark range*, or more simply *benchmark*, is introduced. It is established as follows.² First, the bistatic radar range equation is derived in a manner completely

analogous to that for a monostatic radar. The equation is then solved for the *bistatic maximum range product*, $(R_T R_R)_{\max}$. Next, an *equivalent monostatic maximum range*, $(R_M)_{\max}$, is defined omitting the *max* subscript for convenience, as shown here:

$$R_M = (R_T R_R)^{1/2} \quad (23.1)$$

This equivalent monostatic maximum range, also known as the *geometric mean range*, represents performance of the bistatic radar when transmitter and receiver are co-located; i.e., when $L = 0$. It is defined as the bistatic radar's *benchmark range*. Since this benchmark is geometry-invariant, it becomes useful when comparing bistatic to monostatic range performance. Finally, an oval of Cassini is established as a function of the baseline range, L , normalized to the benchmark range, R_M . Based on this oval, maximum and minimum detection ranges and the coverage area are calculated, all as a function of R_M . This procedure is also used to define bistatic operating regions.

Range Equation. The radar range equation for CW or coherent pulse radars³⁰ is modified for bistatic operation and then solved for the bistatic maximum range product, $(R_T R_R)_{\max}$:

$$(R_T R_R)_{\max} = \left[\frac{P_{av} t_o G_T G_R \lambda^2 \sigma_B F_T^2 F_R^2}{(4\pi)^3 k T_o F_n (E/N_o) L_T L_R} \right]^{1/2} \quad (23.2)$$

where

- R_T = Transmitter-to-target range (m)
- R_R = Receiver-to-target range (m)
- P_{av} = Transmitted average power (W)
- t_o = Signal observation (or integration) time
- G_T = Transmitting antenna power gain
- G_R = Receiving antenna power gain
- λ = Wavelength (m)
- σ_B = Bistatic radar cross section (m^2)
- F_T = Pattern propagation factor for transmitter-to-target path
- F_R = Pattern propagation factor for receiver-to-target path
- k = Boltzmann's constant [1.38×10^{-23} J/K]
- T_o = Standard temperature [290 K]
- F_n = Receiver noise figure
- E/N_o = Received energy to receiver noise spectral density required for detection
- L_T = Transmitting system losses (>1)
- L_R = Receiving system losses (>1)

Equation 23.2 assumes that a matched filter, or an equivalent matched filter such as a cross-correlator, is used on reception. Equation 23.2 is related to the corresponding monostatic maximum range equation by $R_T R_R = R_M^2$ and $\sigma_M = \sigma_B$, where σ_M is the monostatic radar cross section. For pulsed radar operation, $t_o = n/f_p$, where n is the number of pulses integrated and f_p is the pulse repetition frequency. Also, the signal-to-noise ratio required for detection, $(S/N)_{\text{req}} = E/N_o$ when $B\tau \approx 1$, where B is the receiver bandwidth and τ is the pulse width.

The signal processing time, t_o , is sometimes set by the amount of doppler spreading or velocity-walk, Δf_d generated by a moving target. Specifically, $\Delta f_d = (t_o)^{-1} = B_n$,

where B_n is the noise bandwidth of receiver's predetection filter. In the monostatic case, doppler spreading is

$$(\Delta f_d)_m = [2a_r / \lambda]^{1/2} \quad (23.3)$$

where a_r is the radial component of target acceleration. Equation 23.3 also applies to the bistatic case at small bistatic angles, β , particularly in an *over-the-shoulder* operation, where the target lies near the baseline extended beyond either the receiver or the transmitter (called the *extended baseline*).^{*} However, for larger β —the general case—the radial component, which is aligned with the bisector of the bistatic angle, will be reduced. A rule of thumb for these large β conditions is

$$(\Delta f_d)_b = [a_r / \lambda]^{1/2} \quad (23.4)$$

Equation 23.4 is used to set t_o and hence the noise bandwidth of receiver's predetection filter B_n . Since $(\Delta f_d)_b > (\Delta f_d)_m$, the constraint on bistatic signal processing time is slightly less than the equivalent monostatic time.

As in the monostatic equation, the transmitting and receiving pattern propagation factors, F_T and F_R , each consist of two terms: the propagation factors, F'_T and F'_R , and the antenna pattern factors, f_T and f_R , respectively. The antenna pattern factors are the relative strength of the free-space field radiated by the transmitting and receiving antennas as a function of their pointing angles. These factors are applied whenever the target is not at the peak of a beam.

Propagation factors customarily include the effects of multipath, diffraction, and refraction, with atmospheric absorption effects included in the loss terms. As with a monostatic radar, bistatic radar propagation requires a suitable path from the transmitter to the target and the target to the receiver. In contrast to a monostatic radar, however, propagation effects can be significantly different over the two bistatic paths and must be treated separately. Multipath is the primary example, where the target can be in a multipath lobe on one path and a multipath null on the other, depending on antenna and target altitude and terrain conditions.

When a correlation receiver uses the demodulated direct path RF signal as its reference, that signal is subjected to interference (multipath and RFI), which is different from interference affecting the target echo path. If the correlator operates in its linear region, the echo plus its interference convolved with the reference plus its interference produces the desired echo with full matched-filter gain plus interference with gain reduced by mismatch. These signals add vectorially to modify the pattern-propagation factor. However, if the correlator operates in its nonlinear region, which can frequently happen, cross-products are generated, which reduce the echo's matched-filter gain. The amount of loss depends on the magnitude of the interference and is accounted for in the signal-processing loss term.³¹

Ovals of Cassini. The free space, maximum detection contour of a bistatic radar's benchmark range is a circle of radius R_M , just as in the monostatic case. Such a circle assumes constant radar cross-section and pattern propagation factors, which are scenario- and geometry-dependent. For the general bistatic case, where $L > 0$, the free-space maximum detection contour becomes the familiar oval of Cassini, again

* In the first case, the transmitter illuminates the target over the receiver's shoulder; in the second case, the receiver views the target over the transmitter's shoulder.

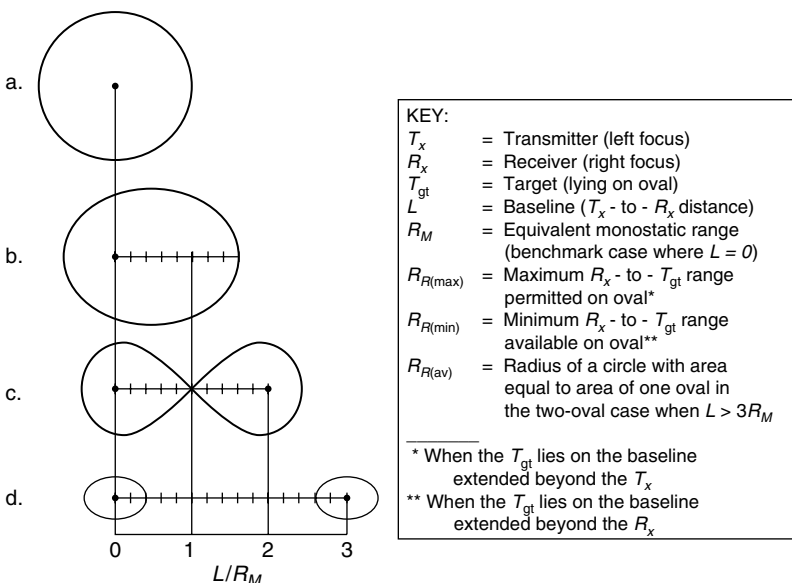


FIGURE 23.2 Normalized ovals of Cassini, lying in the bistatic plane, the plane containing transmitter, receiver, and target² (Courtesy SciTech Inc.)

with the monostatic caveats cited above. Thus, this oval (or ovals) provides a convenient—but at times over-simplified—view of bistatic range coverage and must be used with care.

An additional bistatic caveat is necessary. When the target is on or near the baseline, i.e., located between receiver and transmitter where the bistatic angle $\beta \rightarrow 180^\circ$, a completely different environment is generated: *forward scatter* from both target and clutter. In this case, the target radar cross section (RCS) and clutter scattering coefficient (σ_0) are greatly enhanced, whereas range and doppler measurements are greatly degraded. Often *normal* bistatic operation excludes this region, so that a $10\text{--}20^\circ$ wedge with the apex at the receiver and directed at the transmitter is excised from the oval. Details are given in Willis.¹

Figure 23.2 shows four cases of ovals of Cassini normalized to the benchmark range: (a) benchmark: $L = 0$; (b) one-oval: $L < 2R_M$; (c) lemniscate: $L = 2R_M$; and (d) two-ovals: $L > 2R_M$. In all cases, the transmitter is located at the left oval focus (0). The receiver is located at the right oval focus (0,1,2,3). Other terms and symbols are defined in the key shown with Figure 23.2.

Table 23.1 lists expressions for calculating oval area and maximum/minimum receiver detection ranges for these four cases, again referenced to the benchmark range, R_M .^{*} For Figure 23.2d when $L > 3R_M$, the ovals can conveniently be approximated as circles with radius $R_{R(av)} \sim R_M^2/L$ and corresponding area $\pi R_M^4/L^2$. Expressions for

* The one-oval area formula is derived from Eq. (D.7a) in Willis.¹ It is also used for calculating the lemniscate area. Formulas for the two-oval area are derived from Eq. (D.11a) in Willis.¹ More terms in these series can be used if greater accuracy is required.

TABLE 23.1 Area and Detection Ranges for General Ovals of Cassini² (*Courtesy SciTech, Inc.*)

Case	L	Area (of one oval)	$R_{R(\max)}$ (on R_x oval)	$R_{R(\min)}$ (on R_x oval)
Circle (Benchmark)	0	πR_M^2	R_M	R_M
One Oval	$<2R_M$	$\sim\pi[R_M^2 - L^4/(64R_M^2)]$	$(R_M^2 + L^2/4)^{1/2} + L/2$	$(R_M^2 + L^2/4)^{1/2} - L/2$
Two Ovals	$>2R_M$	$\sim\pi R_M^2 [R_M^2/L^2]$	$L/2 - (L^2/4 - R_M^2)^{1/2}$	$(R_M^2 + L^2/4)^{1/2} - L/2$
	$>3R_M$	$\sim\pi R_M^2 [R_M^2/L^2]$	$\sim R_M^2/L$	$\sim R_M^2/L$

receiver (and transmitter) ranges on the opposite oval are readily calculated through mirror-image symmetry. Also note that the area of every bistatic oval is always less than the monostatic circle.

The expressions in Table 23.1 can also be used to assess first-order bistatic radar line-of-sight (LOS) constraints, where the LOS is defined as a line between transmit and receive antennas tangent to the Earth's surface. Specifically, for a given target, transmitter and receiver altitudes, the target must simultaneously be within LOS to both the transmitter and receiver sites. For a smooth, 4/3 Earth model, the LOS range r_R between a receive antenna of altitude h_R and target of altitude h_t is

$$r_R = 130 (\sqrt{h_R} + \sqrt{h_t}) \quad (23.5)$$

where all units are in kilometers. Similarly, the LOS range r_T between a transmit antenna of altitude h_T and target of altitude h_t is

$$r_T = 130 (\sqrt{h_T} + \sqrt{h_t}) \quad (23.6)$$

Thus, to prevent LOS truncation of the ovals, $r_R \geq R_{R(\max)}$ and $r_T \geq R_{T(\max)}$. These expressions ignore both diffraction and multipath, which can significantly alter these ranges, so they must be considered first-order approximations.

A typical task for bistatic air surveillance is to select a baseline L so that a receiver with antenna altitude h_R will match existing LOS coverage of a transmitter with antenna altitude h_T . For the worst case, over-the-shoulder geometry, the requirement would be to match LOS coverage on the extended baseline, $r_T = r_R + L$, so that

$$L = 130 (\sqrt{h_T} - \sqrt{h_R}) \quad (23.7)$$

For example, when $h_T = 0.1$ km and $h_R = 0.01$ km, $L = 28$ km, which from Eq. 23.5 and 23.6 will provide LOS to an 8.5 m altitude target flying above the extended baseline, 25 km from the receiver and 53 km from the transmitter. Baselines greater than 100 km can pose severe target LOS problems. For example, if $L = 120$ km and $h_T = 0.3$ km, then from Eq. 23.6, the transmitter would only illuminate a target flying directly above the receiver at an altitude $h_t > 0.14$ km. Thus, the target could readily under-fly the illumination, and low-altitude air surveillance capability is lost. As a consequence, the bistatic radar must either employ a greatly elevated (~1 km) transmitter at these long baselines or operate with shorter baselines to achieve acceptable low altitude surveillance coverage. Note that the two-oval case can also require a very high altitude for the site located in the oval not under surveillance—so high that the site must often become airborne.

Finally, the transmit antenna will be in direct LOS of the receive antenna when $L \leq r_T + r_R$ with $h_t = 0$, so that, again with all units in kilometers

$$L \leq 130 (\sqrt{h_T} + \sqrt{h_R}) \quad (23.8)$$

If Eq. 23.8 is satisfied, extraordinary measures are usually required to suppress the direct path signal to a level where targets can be detected, as outlined in Section 23.9.

23.4 APPLICATIONS

Ovals of Cassini can be used to define three operating regions for a bistatic radar, *co-site*, *receiver-centered*, and *transmitter-centered*.¹ Co-site corresponds to Figure 23.2b; receiver-centered to the right oval in Figure 23.2d; and transmitter-centered to the left oval in Figure 23.2d. The type of transmitter—*dedicated*, *cooperative*, or *non-cooperative*—completes the taxonomy. A dedicated transmitter is designed and controlled by the bistatic or multistatic radar, analogous to a monostatic radar. Both cooperative and noncooperative transmitters are transmitters-of-opportunity—designed for other functions, including radar and communications, but found suitable for bistatic operation. The cooperative transmitter is controlled by allied or friendly forces; the noncooperative transmitter, by hostile or neutral forces. Table 23.2 summarizes bistatic radar applications in these operating regions.*

Entries in the dedicated transmitter/co-site category represent a complete bistatic radar suite—radars with all components including the transmitter designed for bistatic operation. Many of these systems were developed, tested, or deployed prior to 1980. Examples are the French, USSR, and Japanese forward scatter fences used in WWII,² the AN/FPS-23 for air-defense gap filling,² PARADOP and MIDOP range-instrumentation trackers,⁹ SPASUR for space surveillance,^{12,32} and Sanctuary for air defense.^{33,34} The BRWL for artillery, mortar, and rocket location,³⁵ the Russian Struna-1 forward scatter fence,³⁶⁻³⁸ and the French Graves for space surveillance³⁹ were later developments.

Omitted entries in the dedicated transmitter column for operation in the receiver- and transmitter-centered ovals at large baseline ranges are dictated by operations and cost: both cooperative and noncooperative transmitters-of-opportunity are often present and capable of supporting bistatic operation in these small areas of interest.

TABLE 23.2 Bistatic Radar Applications

Receiver Operating Regions	Range Relationship	Dedicated Transmitter	Cooperative Transmitter	Noncooperative Transmitter
Co-site	$L < 2 R_M$	<ul style="list-style-type: none"> • Air surveillance • Range instrumentation • Satellite tracking • Intrusion detection 	<ul style="list-style-type: none"> • Air surveillance • Range instrumentation • Ionospheric measurement • Wind measurement 	<ul style="list-style-type: none"> • Air surveillance
Receiver-centered	$L > 2 R_M$ $R_T \gg R_R$		<ul style="list-style-type: none"> • Short-range air surveillance • Silent air-to-ground attack • Planetary exploration 	<ul style="list-style-type: none"> • Short range surveillance
Transmitter-centered	$L > 2 R_M$ $R_R \gg R_T$		<ul style="list-style-type: none"> • Planetary exploration 	<ul style="list-style-type: none"> • Air threat monitoring • Missile launch alert

* A multistatic radar with its requirement for common spatial coverage nearly always operates in the co-site region.

Furthermore, this approach is less costly and when exploiting noncooperative transmitters, more covert and less risky than using a dedicated transmitter. Consequently, dedicated transmitters are not usually considered for these applications.

Entries in the cooperative and noncooperative transmitter columns are called *hitchhikers* when the transmitter is a monostatic radar. When the transmitter is from a communications or broadcast system, i.e., not from a radar, entries are called a *passive bistatic radar (PBR)*.

Examples of a hitchhiker operating with a cooperative transmitter in the co-site region are the *Multistatic Measurement System* operating with *TRADEX* for increasing ballistic missile reentry measurement accuracy^{40,41} and the commercial, Binet Inc., bistatic receiver operating with monostatic doppler weather radars to measure three-dimensional vector wind fields.^{2,42,43} Figure 23.3 is a block diagram of the Binet Inc.-developed prototype.

Examples of hitchhikers operating with a cooperative transmitter in the receiver-centered region are the *Covin Rest* program, operating with the space-shuttle radar for synthetic aperture radar (SAR) ground mapping⁴⁴; the *TBIRD* program operating with *Joint STARS* for silent air-to-ground attack via forward-looking bistatic SAR^{2,45}; and the *BAC* program operating with *AWACS* for alerting and cueing short range, mobile air-defense systems.^{46,47}

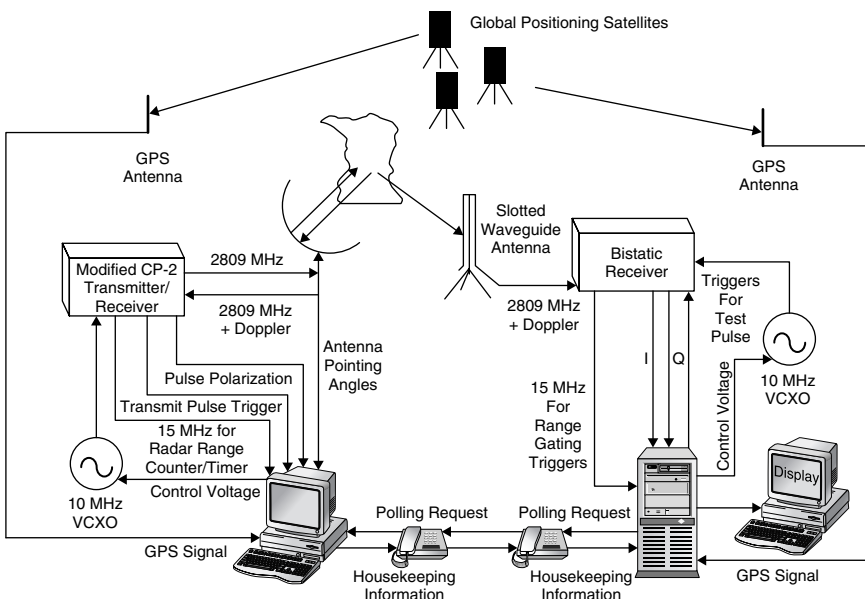


FIGURE 23.3 Simplified block diagram of the Binet Inc.-developed bistatic wind measurement prototype system. A modified CP-2 monostatic weather radar transmits and receives on a narrow beam antenna, while one or more bistatic receive sites 10–20 km from the CP-2 receive bistatically scattered energy from the same illuminated weather volume over a broad antenna beam. A transmit/receive tube is used to protect the receiver, just as in a monostatic radar. All generated frequencies are locked to the master 10-MHz VCXO, which is, in turn, locked to GPS timing signals. Synchronization and other housekeeping data are sent over telephone lines. Signal and data processing is PC-based. (after J. Wurman⁴³ © IEEE 1994)

Hitchhikers using cooperative monostatic radar transmitters also have the inherent capability to counter retro-directive jammers operating against their host radar. Because the jammer uses a high-gain antenna to retro-direct the transmitter's signal back to the transmitter (and thus its monostatic receiver), the spatially separated hitchhiker can be positioned in the sidelobes of that antenna, thus reducing the effectiveness of the jammer. A rule of thumb is to anticipate enhanced hitchhiker performance whenever the bistatic angle is greater than the estimated 3-dB width of the retro-directed main beam.

Examples of PBRs operating with cooperative broadcast transmitters in the co-site region are the *Manastash Ridge Radar* operating with an FM broadcast transmitter for tropospheric soundings,^{2,48} *Silent Sentry* operating with FM and TV broadcast transmitters,^{49,50} and the *HDTV-Based Passive Radar* operating with a high definition-TV broadcast transmitter,⁵¹ the latter two configured for air surveillance. Examples of PBRs operating with cooperative communications transmitters in the receiver- and transmitter-centered regions are bistatic radars for planetary exploration. They use a data link transmitter on the probe vehicle in the transmitter-centered region and an Earth-based command transmitter in the receiver-centered region.^{2,52}

The term cooperative transmitter is somewhat of a misnomer. For example, a cooperative TV or FM station operator would not be inclined to "cooperate" with a PBR by altering antenna coverage or modifying broadcast material with special waveforms. Furthermore, there is always the possibility of a transmitter failure in the course of normal operations or from an enemy attack. This event will degrade performance of a PBR that operates with multiple transmitters and eliminate performance of a PBR that operates only with that transmitter. As a result, the PBR is free to exploit cooperative (or noncooperative) transmissions if they are suitable; however, commerce controls their operation with the PBR remaining a user of opportunity, specifically suffering nonoptimum waveforms (Section 23.9), limited elevation coverage, and occasionally reduced or denied performance.

Constraints also apply when a hitchhiker attempts to exploit a cooperative or non-cooperative monostatic radar, specifically with the hitchhiker suffering antenna scan-on-scan problems (Section 23.9). However, the potential for enhancing performance of a cooperative monostatic radar against retro-directive-type jammers when using a suitably positioned hitchhiker necessitates distinguishing cooperative from noncooperative transmitters.

In the noncooperative transmitter column, if a noncooperative transmitter and a hitchhiker were located in or near a battle area, a hitchhiker could use that transmitter in the co-site region just as it would for a cooperative transmitter. The German *Klein Heidelberg* hitchhiking off the British *Chain Home* radars to conduct air surveillance during WWII is an example.^{53,54} A hitchhiker implanted in or flying over hostile areas could use any high-powered satellite transmitter illuminating that area to conduct short-range surveillance in the receiver-centered oval.

The most significant system to use a dedicated transmitter is the *Space Surveillance (SPASUR)* 217 MHz multistatic radar fence. It was deployed starting in 1958 at seven sites spanning the continental United States to detect and track noncooperative satellites.^{12,32} Transmitters are located at three sites, the largest of which transmits 1 MW CW from a linear array about 3 km long, generating a fixed fan beam. The six receive sites consist of seven or eight linear arrays with dimensions on the order of 1 km, also generating fixed fan beams collinear with the transmit beam. Figure 23.4 shows the data flow in a typical receiving station.¹²

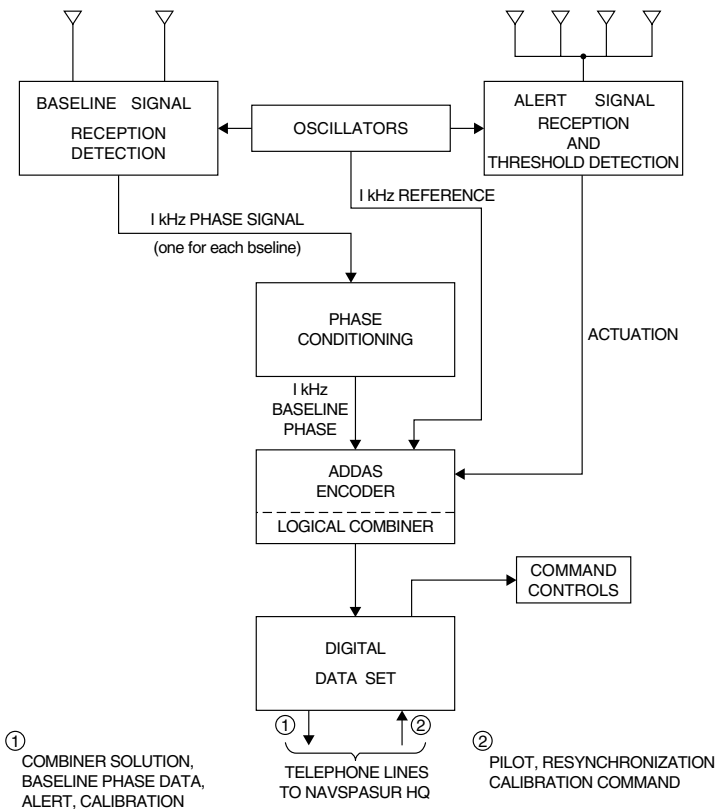


FIGURE 23.4. Real-time data flow in a NAVSPASUR receiving station. “Transmitter energy reflected by the satellite is received by various collinear arrays of dipoles at the receiver station... [Signals] from four in-line arrays feeds the alert receiver which detects the presence of radio energy in excess of preset threshold levels. The reflected energy is also simultaneously received on other arrays that are separated in the east-west direction by various distances (baseline). Signals from any two can be added to form a baseline pair. The baseline receivers employ triple frequency conversion where the phase difference of the signals received by the antenna pair is preserved in a 1000-hertz difference frequency [called a 1 kHz phase signal in the figure]... There is a radio receiver and consequently a 1000-hertz phase [signal] for each baseline pair (12 east west and 3 north south). This phase signal is compared with a 1000-hertz reference signal and encoded (digitized) by the ADDAS encoding equipment. The digital combiner, contained within the ADDAS encoder, receives the 1 KHz phase data and generates an unambiguous zenith angle solution. The combiner outputs along with digitized phase information and control bits, foremost of which is ‘alert,’ are applied to the telephone lines via a digital data transmitter.”(from Handbook for NAVSPASUR System Orientation,¹² courtesy U.S. Navy)

Target location is established by triangulation, i.e., the intersection of zenith angle (DOA) measurements from two or more receive sites. Subsequently a three-site fence in South Texas was deployed to evaluate the use of bistatic range measurements to improve location accuracy,⁵⁵ but it never entered continuous operation.

According to Easton,³² the *SPASUR* design was driven by cost: a 15,000 nmi detection range required very high average power, which was satisfied by the lowest cost CW operation. But this solution, in turn, required separate sites for isolation—hence, multistatic operation. The stationary beam linear arrays also minimized cost when compared to scanning arrays or reflector antennas. In short, fix the beams and let the satellites fly through them. It has been in continuous use since 1958.

A hitchhiker using a cooperative radar transmitter in the co-site region was the *Multistatic Measurement System (MMS)*. It was installed at the U.S. Kwajalein Missile Range in 1980 as an adjunct to the *TRADEX* L band monostatic radar.⁴⁰ *TRADEX* operated in its normal monostatic mode, acquiring, tracking, and illuminating ballistic missile reentry vehicles (RVs). Two unmanned, slaved receive stations, located about 40 km from *TRADEX*, received echoes bistatically scattered off the RV and recorded bistatic range, doppler, and signature data from RVs. This data was used to calculate RV position and dynamics near the atmospheric pierce point or start of re-entry. The system was projected to measure three-dimensional position and velocity with accuracies better than 4 m and 0.1 m/s, respectively, throughout re-entry.⁴³

Field tests showed that MMS range data combined with *TRADEX*'s monostatic range data in a trilateration net provided the most accurate estimate of exo-atmospheric RV positions obtained by any of the range radars. MMS operations were concluded in 1993⁵⁶ after the metric accuracy of monostatic radars was improved.⁵⁷

In the mid-1990s, a PBR using a cooperative FM broadcast transmitter in the co-site region was developed by the University of Washington. Called the *Manastash Ridge Radar (MRR)*, it is designed to study turbulence in the ionosphere, specifically auroral E-region irregularities, using range, doppler, and DOA (via interferometry) measurements.^{2,48} Motivation for MRR development included lower cost, increased safety, spectrum availability, and pedagogical opportunity. MRR provides range-time intensity and range-doppler plots to the World Wide Web every half-hour. Although it is not subject to the stringent air-defense requirements for accurate location of multiple targets in real time, it has detected meteors and aircraft in the course of normal operations.

A second PBR, called the *HDTV-Based Passive Radar*,⁵¹ exploits a cooperative high-definition TV transmitter for air surveillance in the co-site region. It uses range multilateration from four receivers located within 10 km of the transmitter to track low-flying aircraft and helicopters as a gap-filler for monostatic air surveillance radars. Predicted detection and tracking ranges of 30 km on a 1 m² target have been demonstrated in real time with 2D tracking errors generally less than 50 m. Coarse target elevation has also been measured. Doppler data has been used to resolve *ghosts*, i.e., false detections that inevitably arise when using multilateration on unaugmented targets.²

PBRs have used satellite communication transmitters to measure characteristics of moon and planetary surfaces and atmospheres in both the transmitter- and receiver-centered regions. The first successful piggyback operation in 1967 exploited data link signals transmitted from the *Luna-11* probe, scattered off the moon's surface, and then received by an Earth-based station, in a down-link mode characterized by the transmitter-centered oval of Cassini. Such stations include the Arecibo Observatory and the NASA Deep Space Network. Subsequent measurements were made using *Lunar Orbiter-1*, *Explorer-35*, and *Apollo 14-16*. Mars bistatic radar measurements were made using *Mariner-6*, -7, *Viking-1*, -2, *Mars Global Surveyor*, and *Mars Express*. Venus measurements were made by *Veneras-9*, -10, *Magellan*, and *Venus Express*.^{2,52} Figure 23.5 is a simplified schematic of an Earth-based receiver.²

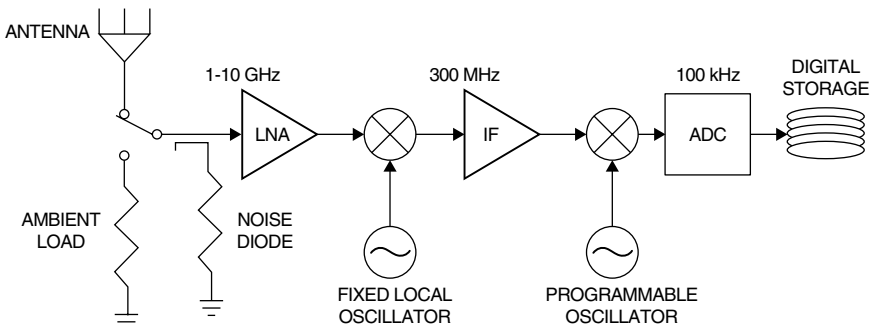


FIGURE 23.5. Block diagram of a typical Earth-based system used for downlink bistatic radar. The low-noise amplifier (LNA) is either a cooled maser or a field effect transistor and may be switched between the antenna and an ambient load, allowing amplitude calibration of the input. During bistatic operations, a signal from the low-level noise diode, previously calibrated against the ambient load, may be injected to monitor real-time performance of the system. Microwave inputs (1–10 GHz) are mixed to a 300 MHz intermediate frequency (IF) for amplification. A programmable oscillator, which can correct for first-order doppler effects, then mixes the IF signal to baseband, and digital samples are stored for later processing. Although an analog-to-digital conversion is shown at the output, the ADC may actually take place at any point in the system.² (Courtesy SciTech)

A reciprocal but more complex and costly uplink mode uses a bistatic receiver carried by the probe, collecting high power, Earth-transmitted command signals first scattered off the planet's surface and characterized by the receiver-centered oval of Cassini. It has an ~ 30 dB greater link margin, which was first used for Mars Odyssey and is planned for future probes. In both configurations, even though two legs of the bistatic triangle are extraordinarily long ($>10^5$ miles), the third leg is sufficiently short (~ 10 miles) to produce strong echoes at the receiver.²

These piggyback bistatic radars have provided useful data in simple, inexpensive surveys of planetary surface properties as a prelude to robotic or human exploration, specifically centimeter- to meter-scale roughness and material densities in the top few centimeters of regolith. Special geometries, such as near-backscatter to identify deposits of clean water ice, are also a unique advantage of bistatic radar. The ability to observe forward scattering at latitudes away from planetary equators is also advantageous for probing surface characteristics.

23.5 BISTATIC DOPPLER

Figure 23.6 defines the geometry for bistatic doppler when the target, transmitter, and receiver are moving. The target has a velocity vector of magnitude V and aspect angle δ referenced to the bistatic bisector. The transmitter and receiver have velocity vectors of magnitude V_T and V_R and aspect angles δ_T and δ_R , respectively, referenced to the north coordinate system of Figure 23.1. All vectors are projections of the three-dimensional vectors onto the bistatic plane.

Target Doppler. When the transmitter and receiver are stationary ($V_T = V_R = 0$), the target's bistatic doppler at the receive site f_B is

$$f_B = (2V/\lambda) \cos \delta \cos (\beta/2) \quad (23.9)$$

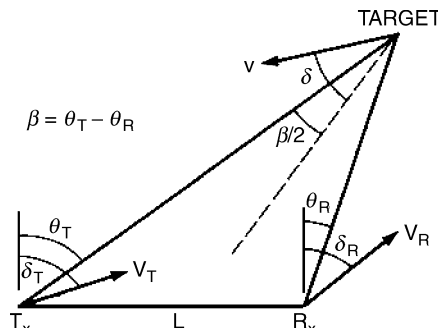


FIGURE 23.6 Geometry for bistatic doppler in the bistatic plane

The term f_B also defines the *doppler beat frequency*, which is produced by mixing the target's doppler with the direct path signal in the receiver. Willis¹ provides an expression for f_B when all three sites are in motion. Equation 23.9 shows that

- When $\beta=0^\circ$, f_B reduces to the monostatic case for a monostatic radar located on the bistatic bisector. The magnitude of the bistatic doppler is never greater than that of this monostatic doppler.
- When $\beta=180^\circ$, $f_B=0$ for any δ , which is the forward-scatter case.
- When $\delta=\pm 90^\circ$ the bistatic doppler is zero. Since these velocity vectors are also tangent to a range-sum ellipse at this point, all such ellipses (including the baseline) become contours of zero target doppler.
- When $\delta=0^\circ$, the bistatic doppler is a maximum. Since this velocity vector is also tangent to a hyperbola orthogonal to the range-sum ellipse at this point, all such hyperbolae become contours of maximum target doppler.
- When $\delta=\pm \beta/2^\circ$, the velocity vector is pointed at the transmitter or receiver and $f_B=(2V/\lambda) \cos^2(\beta/2)$, which occasionally appears in the literature as a special case of Eq. 23.9.

If a monostatic radar is located at the transmit site and a bistatic hitchhiker is located at the receive site, both measuring target doppler, f_M and f_B , respectively, the two measurements can be combined to estimate the target velocity vector (V, δ) in the bistatic plane. One such estimate is

$$\delta = \tan^{-1} \{ [f_M / f_B \sin(\beta/2)] - \cot(\beta/2) \} \quad (23.10)$$

$$V = \lambda f_B / 2 \cos \delta = \lambda f_M / 2 \cos(\delta - \beta/2) \quad (23.11)$$

where β is obtained by solving the bistatic triangle, for example, by using monostatic range, monostatic LOS, and an estimate of the baseline. A third hitchhiking site allows the target velocity vector to be measured in three dimensions. This process is called *dual-doppler* for two measurements and *multiple-doppler* for three or more measurements, and has been used to measure three-dimensional vector wind fields.^{2,42,43,58}

Isodoppler Contours. When the target is stationary and the transmitter and receiver are moving (e.g., on airborne platforms), the bistatic doppler shift at the receiver site f_{TR} is

$$f_{TR} = (V_T/\lambda) \cos(\delta_T - \theta_T) + (V_R/\lambda) \cos(\delta_R - \theta_R) \quad (23.12)$$

where terms are defined in Figure 23.6.

The locus of points for constant doppler shift on the Earth's surface is called an *isodoppler contour*, or *isodop*. Clutter returns are characterized by these isodops, which are called *clutter doppler shift*. In the monostatic case and a flat Earth, these isodops are conic sections in three dimensions and radial lines emanating from the radar in two dimensions. Because these isodops are aligned with the radar's look angle, the clutter is called *stationary*. In the bistatic case, the isodops are skewed away from the look angle, depending upon the geometry and platform motion, and the clutter is called *nonstationary*. Bistatic isodops are developed analytically for two dimensions and a flat earth by setting $f_{TR} = \text{constant}$ in Eq. 23.12 and solving for θ_R (or θ_T , if appropriate).

Figure 23.7 is a plot of bistatic isodops in a two-dimensional bistatic plane, i.e., where the transmitter and receiver are at zero or near-zero altitude, for the following conditions: $V_T = V_R = 250 \text{ m/s}$, $\delta_T = 0^\circ$, $\delta_R = 45^\circ$, and $\lambda = 0.03 \text{ m}$.

Dimension of the grid on the bistatic plane is arbitrary; that is, the isodops are invariant with scale. On the left and right sides of Figure 23.7, the isodops are approximately stationary, which are pseudo-monostatic operating points. Elsewhere, the isodops are nonstationary. In these nonstationary regions, the quality of bistatic SAR imagery is limited and moving target indication (MTI) performance is degraded when using standard monostatic radar processing techniques.

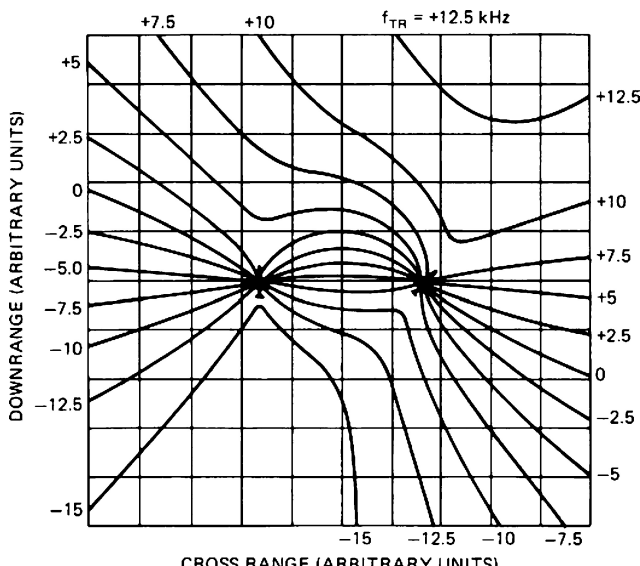


FIGURE 23.7 Bistatic isodoppler contours for two dimensions and a flat earth (Courtesy Lee R. Moyer, Technology Service Corp.)

Research was started in the 1990s to improve the quality of bistatic SAR images, which were constrained to coherent integration times of a few seconds¹ and consequently were of limited tactical interest. Specifically, local oscillator phase instabilities were reduced and bistatic automatic focusing (*autofocus*) algorithms were developed to improve range measurement accuracy from the antenna phase center to the imaged scene. Bistatic autofocus requires that the position of both transmit and receive platforms must be tracked with subwavelength relative accuracy to correct time-varying phase errors as part of the image formation process. The result allowed an increase in coherent integration times comparable to monostatic SAR, typically >10 seconds. Consequently, bistatic SAR image quality was greatly improved, as reported by B. Rigling in Chapter 10 of Willis and Griffiths.²

Bistatic space-time adaptive processing (STAP) was also developed to improve MTI performance of separately moving transmit and receive platforms. Since bistatic clutter exhibits nonstationary space-time characteristics, bistatic STAP methods are not simple applications of monostatic approaches, but a new class of algorithms. Specifically, they apply a data-dependent weighting to voltages collected over multiple receive antenna channels and pulses. This weighting dynamically tailors a filter response in angle and bistatic doppler to suppress ground clutter reflections. Digital beamforming^{59,60} is required for this operation. Other necessary elements include a means to estimate the spatio-temporal clutter covariance matrix (the data-dependent element of the filter weighting) and hypothesis of the target steering vector. In general, auxiliary data taken from range bins other than the cell under test is used to estimate the unknown, but critical, clutter covariance matrix. With compensation for nonstationary behavior, bistatic clutter suppression has been greatly improved, as reported by W. Melvin in Chapter 11 of Willis and Griffiths.²

23.6 TARGET LOCATION

Bistatic Location. A bistatic receiver typically uses range sum ($R_T + R_R$) for target location, which can be estimated by two methods. In the direct method, the receiver measures the time interval ΔT_{rt} between reception of the transmitted signal and reception of the target echo. It then calculates the range sum as $(R_T + R_R) = c\Delta T_{rt} + L$. This method can be used with any suitable modulated transmission and any type of transmitter (dedicated, cooperative, or noncooperative), given an adequate LOS between transmitter and receiver. In the indirect method, presynchronized stable clocks are used by the receiver and a dedicated transmitter. The receiver measures the time interval ΔT_{tt} between the transmission of a signal and reception of the target echo. It then calculates the range sum as $(R_T + R_R) = c\Delta T_{tt}$. A transmitter-to-receiver LOS is not required unless periodic clock synchronization is implemented over the direct path.

The traditional method for converting target range sum into target range from the receiver, R_R , is¹³

$$R_R = \frac{(R_T + R_R)^2 - L^2}{2(R_T + R_R + L \sin \theta_R)} \quad (23.13)$$

The baseline L can be determined using GPS or other methods such as an emitter locator for noncooperative transmitters. As outlined in Section 23.2, the receiver look angle, θ_R , can be measured directly with a phased array antenna that scans in two dimensions,

or target azimuth and elevation measurements can be converted to θ_R .¹ Beam-splitting techniques can be used to reduce the measurement error. Even with beam-splitting, θ_R is the critical parameter establishing accuracy of the R_R estimate, since, as in the monostatic case, its error is proportional to target range. A full error analysis of Eq. 23.13 is given in Section 5.2 of Willis.¹ No bistatic radar operating autonomously has been shown to provide adequate location of air or space targets without employing receive apertures comparable in size to monostatic receive apertures used for those purposes.

In the special case of a bistatic radar using the direct range sum estimation method, when $R_T + R_R \approx L$ Eq. 23.13 can be approximated as¹

$$R_R = \frac{c\Delta T_{\text{rt}}}{1 + \sin \theta_R} \quad (23.14)$$

Two examples are a receiver operating in an over-the-shoulder geometry and the transmitter operating on a satellite with the receiver and target near the earth. The error in Eq. 23.14 is less than 10 percent for $0^\circ < \theta_R < 90^\circ$ and $L > 0.82 (R_T + R_R)$ or $4.6 c\Delta T_{\text{rt}}$. The error grows rapidly for $\theta_R < 0^\circ$.

Other target location techniques are possible.^{13,14,18,29,61-64} For example, when a bistatic hitchhiker exploits the transmitter of a monostatic radar, the radar's look angle θ_T can be used in place of or in conjunction with θ_R . An example of the latter is the *theta-theta* location technique, where

$$R_R = L \cos \theta_T / \sin (\theta_T - \theta_R) \quad (23.15)$$

and $\theta_T - \theta_R = \beta$. A dedicated or cooperative monostatic radar can provide values of θ_T directly to the hitchhiker. Otherwise, the hitchhiker must estimate the value, for example, via an emitter locator measuring the radar's antenna scan rate when it is predictable. In this case, target location accuracy is often set by the θ_T estimation error.

Multistatic Location.^{9,14,65} Multistatic location typically uses multiple transmitters operating with one receiver or multiple receivers operating with one transmitter. Ellipses of constant range-sum, i.e., isorange contours, from each transmitter-receiver pair are calculated and combined at a central site to produce intersecting contours, which locate the target.* Multistatic cross-range location can be more accurate than monostatic or bistatic cross-range location since angle data, with its range-dependent accuracy, is not used. The multistatic radar must, however, use multiple, properly located sites with both overlapping coverage and simultaneous measurements, which, in turn, require broad transmit and receive beams to achieve this accuracy. These requirements usually combine to restrict multistatic air surveillance performance to short or medium ranges.

Geometric dilution of precision (GDOP) establishes multistatic location accuracy (and resolution) and is developed by D. Barton in Chapter 6 of Willis and Griffiths.² GDOP is a function of the angle of intersection, α , between isorange contours. Because the bisector of a bistatic angle is orthogonal to an isorange contour, GDOP can readily be determined by the angle of intersection, also α , of these bistatic bisectors. In the simplest case, the down-range error σ_{dr} is proportional to $[\sqrt{2} \cos (\alpha/2)]^{-1}$ and cross-range error σ_{cr} is proportional to $[\sqrt{2} \sin (\alpha/2)]^{-1}$.

* Isorange contours intersect at other locations as well. These nontarget locations are called *ghosts*, which must be excised. This subject is treated in Chapter 6 of Willis and Griffiths.²

For example, when the target is surrounded on three sides by a receive site, a transmit site, and another receive site such that $\alpha = 90^\circ$, $\sigma_{dr} = \sigma_{cr} = 1$. This geometry represents the optimum case of a unity GDOP factor, yielding a circular error ellipse with radius equal to the range error of one transmit-receive pair. In contrast, when the target is located some distance from the three sites, α is reduced. For example, when $\alpha = 5^\circ$, $\sigma_{dr} = 0.71$, and $\sigma_{cr} = 16.2$. Thus, the down-range error is slightly reduced but the cross-range error is greatly increased, not unlike that of a radar using angle data to establish cross-range accuracy.

These examples also apply when ground-based multistatic sites attempt to measure target altitude. When the sites surround the target, for example, when positioned around the launch site of a ballistic missile, α remains relatively large during the missile's launch phase, yielding precise altitude estimates. When the sites are some distance from the target, for example, when conducting air or missile surveillance, α is small, yielding poor altitude estimates.

Both bistatic and multistatic radars can potentially achieve even better location accuracy by using narrow-band doppler tracking under the following conditions: (1) When integrating doppler data, initial conditions (the pesky constant of integration) can be established with sufficient accuracy. (2) When taking sequential doppler measurements, the target's velocity vector remains constant⁶⁴ or predictable.⁶² For example, many doppler-only, precision range instrumentation systems were developed in the U.S. after WWII.⁹ Both beacon-aided and skin-track systems were developed. All required initialization of the track data, which was conveniently provided by the target's launch coordinates. However, if the target return momentarily faded or the transponder signal was interrupted during flight so that track was lost, there was no way to reinitialize new track data and subsequent location estimates became biased or were lost. These systems were subsequently replaced with precision monostatic radars and optical trackers.

23.7 TARGET CROSS SECTION^{14,15,30,66-87}

The bistatic radar cross section (RCS) of a target σ_B is a measure, as is the monostatic radar cross section σ_M , of the energy scattered from the target in the direction of the receiver. Bistatic cross sections are more complex than monostatic cross sections in the optical region since σ_B is a function of aspect angle and bistatic angle β .^{*} Three bistatic RCS regions are of interest in the optical region: pseudo-monostatic, bistatic, and forward scatter. Each region is defined by the bistatic angle. The extent of each region is set primarily by the target's physical characteristics.

Pseudo-Monostatic RCS Region. The Crispin and Siegal monostatic-bistatic equivalence theorem applies in the pseudo-monostatic region⁶⁹: for vanishingly small wavelengths, the bistatic RCS of a sufficiently smooth, perfectly conducting target is equal to the monostatic RCS measured on the bisector of the bistatic angle. Sufficiently smooth targets include spheres, elliptic cylinders, cones, and ogives, allowing the region to extend out to $\beta = 40^\circ$ and occasionally out to $\beta = 90^\circ$.^{1,76-79}

* However in the resonance region, typically at VHF and low UHF for many air targets, variations in $\beta < \sim 90^\circ$ have little effect on σ_B , such that $\sigma_B \approx \sigma_M$.²

For targets of more complex structure, the extent of the pseudo-monostatic region is reduced. A variation of the equivalence theorem developed by Kell⁷⁴ applies to small bistatic angles, in some cases as small as 5°: the bistatic RCS of a complex target is equal to the monostatic RCS measured on the bisector of the bistatic angle at a frequency lower by a factor of $\cos(\beta/2)$.

Kell's complex targets are defined as an assembly of discrete scattering centers (simple centers such as flat plates, reflex centers such as corner reflectors, skewed reflex centers such as a dihedral with corner $\neq 90^\circ$, and stationary phase regions for creeping waves). When the wavelength is small compared to target dimensions, these complex target models approximate conventional aircraft, ships, ground vehicles, and some missiles. The targets can be composed of conducting and dielectric materials.

At small bistatic angles, the $\cos(\beta/2)$ frequency reduction term has little effect in Kell's pseudo-monostatic region. For example, a 10° bistatic angle corresponds to a 0.4% shift in wavelength and usually can be ignored. Both versions of the equivalence theorem are valid when the positions of the transmitter and receiver are interchanged, given that the target-scattering media are reciprocal. Most media are reciprocal. Exceptions are gyrotropic media, such as ferrite materials and the ionosphere.

Bistatic RCS Region. The bistatic angle at which the equivalence theorem fails to predict the bistatic RCS identifies the start of the second bistatic region. In this region, the bistatic RCS diverges from the monostatic RCS. Kell⁷⁴ identified three sources of this divergence for complex targets and for a target aspect angle fixed with respect to the bistatic bisector. These sources are (1) changes in relative phase between discrete scattering centers, (2) changes in radiation from discrete scattering centers, and (3) changes in the existence of centers—appearance of new centers or disappearance of those previously present.

The first source is analogous to fluctuations in monostatic RCS as the target aspect angle changes, but now the effect is caused by a change in bistatic angle.⁸⁷ The second source occurs when, for example, the discrete scattering center, including flat plates, retro-reflects energy toward the transmitter, and the receiver is positioned outside the retro-reflected beamwidth; thus, the received energy is reduced. The third source is typically caused by shadowing, for example, by an aircraft fuselage blocking one of the bistatic paths—transmitter or receiver LOS to a scattering center.

In general, this divergence results in a bistatic RCS lower than the monostatic RCS for complex targets. For example, Ewell and Zehner⁸¹ measured the monostatic and bistatic RCS of coastal freighters at X band when both the transmitter and the receiver were near grazing incidence. The data was plotted as a ratio of bistatic to monostatic RCS, σ_b/σ_m . The measurements generally match Kell's model: of the 27 data points, 24 show bistatic RCS lower than monostatic RCS. The reduction in bistatic RCS starts between $\beta = 5^\circ$ and $\beta = 10^\circ$ and trends downward to $\sigma_b/\sigma_m = -15$ dB at $\beta = 50^\circ$.

This rather severe loss was measured under special conditions: low grazing angles for targets with vertical surfaces, and dihedrals and trihedrals, which generate a large monostatic RCS. Thus, the bistatic RCS becomes significantly lower as the bistatic angle increases due to shadowing and loss of these speculars and retro-reflectors. Bistatic losses should not be as severe for targets with blended surfaces and a less complex structure, such as combat aircraft.

Glint Reduction in the Bistatic RCS Region. A second effect can occur in the bistatic region. When the bistatic RCS reduction is caused by a loss or attenuation of

large discrete scattering centers, for example, through shadowing, target glint is often reduced. Target glint is the angular displacement in apparent phase center of a target return and is caused by the phase interference between two or more dominant scatters within a radar resolution cell. As the target aspect angle changes, this phase interference changes, shifting the apparent phase center, often with excursions beyond the physical extent of the target. These excursions can significantly increase the errors in angle tracking or measurement systems. When the returns from dominant scatterers are reduced in the bistatic region, the source and hence the magnitude of glint excursions is reduced. Measurements with tactical aircraft showed that for a 30° bistatic angle, peak glint excursions could be reduced by a factor of 2 or more, with most of the excursions contained within the physical extent of the target.⁸⁸ This reduction can be exploited in a semi-active homing missile by modifying its trajectory to maintain $\beta > 20\text{--}30^\circ$ during endgame.

Forward-Scatter RCS Region. The third bistatic RCS region, forward scatter, occurs when the bistatic angle approaches 180°. When $\beta = 180^\circ$ Siegel⁶⁶ showed, based on physical optics, that the forward-scatter RCS, σ_F , of a target with silhouette (or shadow) area A is

$$\sigma_F = 4\pi A^2/\lambda^2 \quad (23.16)$$

where λ , the wavelength, is small compared with the target dimensions. The targets can be either smooth or complex structures and, from the application of Babinet's principle, can be totally absorbing.^{70,75}

For $\beta < 180^\circ$, the forward-scatter RCS rolls off from σ_F . The rolloff is approximated by treating the shadow area A as a uniformly illuminated antenna aperture. The radiation pattern of this *shadow aperture* is equal to the forward-scatter RCS rolloff when $(\pi - \beta)$ is substituted for the angle off the aperture normal. A sphere of radius a will roll off 3 dB at $(\pi - \beta) \approx \lambda/\pi a$, when $a/\lambda \gg 1$. The roll-off continues approximating $J_0(x)/x$ down to $\beta \approx 130^\circ$, where J_0 is a Bessel function of zero order. A linear aperture of length D , with aspect angle orthogonal to the transmitter LOS, will roll off 3 dB at $(\pi - \beta) = \lambda/2D$, when $D/\lambda \gg 1$. The forward-scatter RCS rolloff continues, with sidelobes approximating $\sin x/x$ over the forward-scatter quadrant ($\beta > 90^\circ$).³⁰ For other aspect angles and targets with complex shadow apertures, calculation of the forward-scatter RCS rolloff usually requires simulation.

The forward-scatter RCS of more complex bodies has been simulated and measured; the bodies were both reflecting and absorbing.^{67,70,71,76,82,84-86} Figure 23.8 shows a method-of-moments simulation of a 16- by 1.85-cm cylinder with 992 facets at 35 GHz, for three fixed transmitter-to-target geometries: (a) near end on, (b) 45° aspect angle, and (c) broadside.⁸⁴ All three bistatic regions are shown in the figure. In the broadside geometry, the pseudo-monostatic region occurs at $\beta < 20^\circ$, bistatic at $20^\circ < \beta < 140^\circ$, and forward scatter at $\beta > 140^\circ$. The other two geometries show a similar but broader forward-scatter lobe, as is expected since the silhouette area and hence the shadowing aperture are smaller. The 45° aspect geometry is of interest because the RCS in the bistatic regions is larger than the monostatic RCS for most bistatic angles. The large spike at $\beta = 90^\circ$ is the bistatic specular lobe, analogous to the monostatic specular lobe in the broadside geometry. While Figure 23.8 shows the clear dependency of bistatic RCS on both aspect and bistatic angles, it also serves to caution against attempts to use oversimplified bistatic RCS models, especially in the bistatic region.

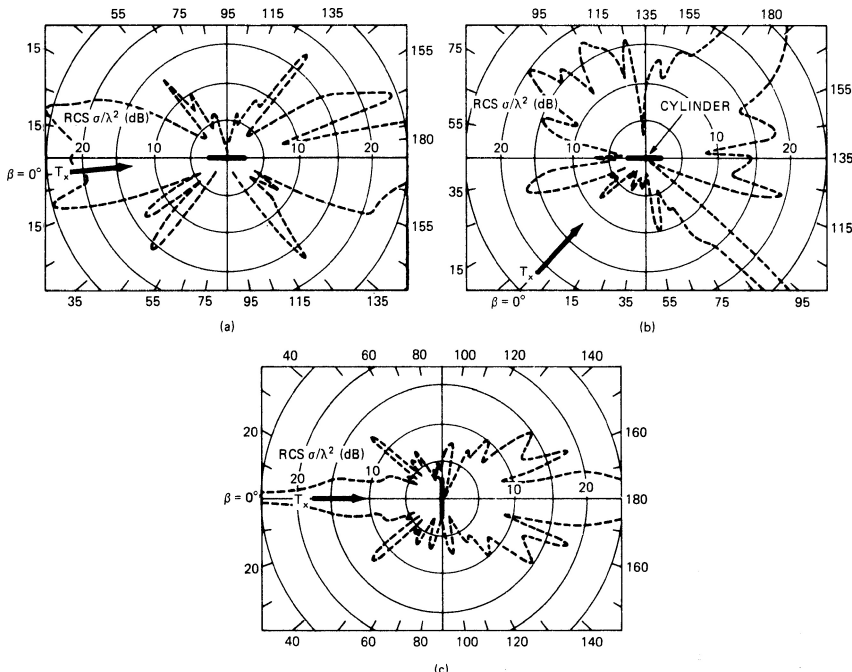


FIGURE 23.8 Simulated bistatic RCS, replotted as a function of bistatic angle for a conducting cylinder, 16 by 1.85 cm at 35 GHz, HH polarization (after R. C. Paddison et al.⁸⁴): (a) near end on, (b) 45° aspect angle, and (c) broadside

23.8 SURFACE CLUTTER

The bistatic radar cross section of surface clutter, σ_c , is a measure, as is the monostatic radar clutter cross section, of the energy scattered from a clutter cell area, A_c , in the direction of the receiver. It is defined as $\sigma_c = \sigma_B^0 A_c$, where σ_B^0 is the scattering coefficient, or the clutter cross section per unit area of the illuminated surface. The clutter cell area A_c has been developed for beam- and range-limited cases and is reported elsewhere.^{1,2} Doppler-limited cases are a function of platform motion, which, in turn, depend on a specific scenario. Consequently, they are modeled on a case-by-case basis.

Bistatic Scattering Coefficient. Values of the scattering coefficient σ_B^0 vary as a function of the surface composition, frequency, and geometry and are obtained through field measurement programs. In 1981, M. M. Weiner⁸⁹ documented and evaluated all unclassified measurements of σ_B^0 ; however, its use was restricted to U.S. government agencies. In 1990, Willis used Weiner's references to reconstruct and evaluate typical data from Weiner's work,⁸⁹ which became available for public use in Willis.^{1,16} In 2003, Weiner's work⁸⁹ was cleared for public release, making available in one document all unclassified σ_B^0 data and analysis through 1980. Weiner then updated his work with data available through 2005 and republished it in Chapter 9 of Advances in Bistatic Radar.² This section summarizes and comments on essential elements of Weiner's work.

The available database for terrain and sea clutter at microwave frequencies consists of nine measurement programs, which are summarized in Table 23.4. The measurement angles shown in Table 23.3 are defined in Figure 23.9, which is a clutter-centered coordinate system similar to those used in all the measurement programs. Because terrain and sea are reciprocal media, θ_i and θ_s are interchangeable in the subsequent data.

Two measurement sets are of interest: in plane, where $\phi = 180^\circ$, and out of plane, where $\phi < 180^\circ$. When $\phi = 180^\circ$, $\beta = |\theta_s - \theta_i|$. In the monostatic case, $\phi = 180^\circ$, $\beta = 0$, and $\theta_s = \theta_i$. In-plane data is shown in bold type on the table.

Out-of-plane data is often used in scatter jamming (*hot clutter*) calculations.

The bistatic angle is calculated from the angles in Figure 23.9 by the use of direction cosines:

$$\beta = \cos^{-1} (\cos \theta_i \cos \theta_s - \sin \theta_i \sin \theta_s \cos \phi) \quad (23.17)$$

Trends in this bistatic scattering coefficient database are summarized from Willis,¹ Weiner,⁸⁹ and Chapter 9 in Willis and Griffiths² as follows:

- Most of the σ_B^0 database is at X band, with 439 out of 650 data curves for both terrain and sea clutter taken by 7 of the 9 organizations. The remaining database consists of 172 data curves at L band (terrain only), 15 at S band (terrain only), 7 at C band (sea only), and 17 at K_a band (terrain only), each provided by one organization. No data is available at VHF or UHF. Thus only X band allows choices in selecting data. The Cost/Peake^{90,91} and Domville^{94–96} in-plane data show good correlation.^{1,108}
- Attempts to model σ_B^0 data have been made using geometrical, statistical, and semi-empirical techniques, including variations of those used to model monostatic data. Meaningful results have only been achieved over a narrow range of in-plane data ($\phi = 180^\circ$).
- Values of σ_B^0 for $\phi > \sim 140^\circ$ are not appreciably different (within ~ 5 dB) from the monostatic case.
- Values of σ_B^0 in a broad angular region centered on $\phi = 90^\circ$ are significantly lower than elsewhere and typically 10 to 20 dB below the monostatic value; consequently, bistatic radar surveillance can be enhanced and hot clutter can be reduced in these regions.
- Values of σ_B^0 are significantly larger near the forward-scattered, specular direction ($\phi = 0^\circ$, $\theta_i = \theta_s$) than elsewhere and may, in some cases, reduce advantages of the enhanced, forward-scattered target RCS, particularly at frequencies > 300 MHz.
- The bistatic-monostatic equivalence theorem used to model the RCS of some targets is not generally useful for clutter modeling, except to indicate an upper limit to σ_B^0 in some regions.

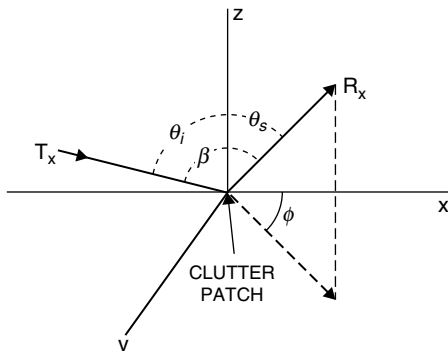


FIGURE 23.9 Coordinate system for bistatic clutter measurements: θ_i = incident angle (in xz plane); θ_s = scattering angle (in plane containing z axis); and ϕ = out-of-plane angle (in xy plane)

TABLE 23.3 Summary of Measurement Programs for Bistatic Scattering Coefficient, σ_B^0 (In-plane data is shown in bold type—see subsequent text.)
 (after M. M. Weiner; Chapter 9,² courtesy SciTech)

Year reported ^{Ref}	Organization	Author	Surface Composition	# Data Curves / Figures	Frequency (GHz)	Polarization	Measurement Angles (degrees)		
							θ_t	θ_s	ϕ
1965 ⁹⁰	The Ohio State University Antenna Lab.	Cost, Peake	Smooth sand Loam Foliage, soybean Rough sand Loam with stubble Grass	10 179 / 32	10	VV HH HV 20 – 80	60 – 85 20 – 80	60 – 85 0 – 85	0 – 145 0, 180
1968 ⁹¹	Johns Hopkins Univ. (APL)	Pidgeon	Sea (sea states 1, 2, 3)	7 / 1	C band	VV VH	87 – 89.9	0 – 80	180
1967 ⁹³	GEC Electronics Ltd., England	Domville	Sea (Beaufort wind 5)	1 / 1	X band	HH	82 – 89	45 – 78	180
1967 ⁹⁴			Rural land		X band	VV	0 – 90	0 – 90	0, 165, 180
1968 ⁹⁵			Urban land						
1969 ⁹⁶			Forest						
			Sea	77 / 4	X band	VV HH	0 – 90	0 – 90	0, 165, 180
			Semi-desert, wet		X band	VV HH	0 – 90	0 – 90	0, 165, 180

TABLE 23.3 Summary of Measurement Programs for Bistatic Scattering Coefficient, σ_b^0 (In-plane data is shown in bold type—see subsequent text.)
(after M. M. Weiner, Chapter 9,² courtesy SciTech) (Continued)

Year reported ^{Ref}	Organization	Author	Surface Composition	# Data Curves / Figures	Frequency (GHz)	Polarization	Measurement Angles (degrees)		
							θ_i	θ_g	ϕ
1977 ⁹	The University of Michigan (ERIM)	Larson, Heimiller, et al.	Grass with cement taxiway	16 / 8	1.3, 9.4	HH HV	50 – 80 70, 75, 80	85 80	0 – 105 0 – 180
1978 ⁹⁸			Weeds and scrub trees	10 / 5	1.3, 9.4	HH HV	50 – 80 60, 70, 80	85 60 – 84	0 – 105 0 – 180
1979 ⁹⁹			Orchard, weeds, scrub trees w/ snow cover	146 / 146	1.3, 9.4	HH HV	60 – 80	60 – 80	0 – 180
1979 ¹⁰⁰	Raytheon Co., Wayland, MA	Cornwell, Lancaster	Beach and sand dunes Sea (sea state 2)	None	9.1	VV	Low graz. angle	Low graz. angle	0 ($\beta \equiv 180^\circ$)
1982 ¹⁰¹	Georgia Inst. of Tech. EES	Ewell, Zehner	Sea (0.9-m, 1.2–1.8-m wave heights)	7 / 7	9.38	VV HH	Low graz. angle	Low graz. angle	95 – 157
1984 ¹⁰²									
1988 ¹⁰³	The University of Michigan EE / CS Dept.	Ulaby et al.	Visually smooth sand Rough sand Gravel	17 / 10	35	VV HH VH HV VH HV	66 60 60	66 60 10 – 80	0 – 170 0 – 170 0 – 90
1992 ¹⁰⁴	MIT Lincoln Lab., MA	Kochanski	Sea (sea state 1)	3 / 3	10	VH VV	89.7	50 – 85	180
1994 ¹⁰⁵	Northeastern Univ., MA	McLaughlin et al.	Forested hills	15 / 15	S band	VV HH	Low graz. angle	Low graz. angle	20 – 70
1995 ¹⁰⁶	Northeastern Univ., MA				S band	VH HV			20 – 70
2002 ¹⁰⁷	Univ. of MA				2.71	Fully polar			28 – 66

In addition to this database, bistatic reflectivity measurements have been made at optical¹⁰⁹ and sonic¹¹⁰ wavelengths and of buildings,¹¹¹ airport structures,¹¹² and planetary surfaces.^{2,52} In each of these measurements, the reflectivity data is expressed in terms of reflected power, not σ_B^0 .

23.9 UNIQUE PROBLEMS AND REQUIREMENTS

In the previous edition of this book, this section covered such hardware problems as time and phase synchronization between transmitter and receiver constrained by technology available in the 1980s. Phase stability was also an issue. Since then massive advances in digital signal correlation and processing, coupled with great reductions in the cost of hardware to execute such processing, have mitigated these problems. Many recent bistatic radar programs have demonstrated quite adequate synchronization and stability—as well as detection performance—using off-the-shelf, commercial hardware. Notable examples are the NATO air defense trials^{2,113,114} and the University of Washington’s *Manastash Ridge Radar* measuring ionosphere turbulence^{2,48}—both passive bistatic radars exploiting FM broadcast transmitters; the *HDTV-Based Passive Radar* exploiting a high definition-TV broadcast transmitter for air surveillance^{2,51}; the inexpensive, commercial bistatic receiver hitchhiking off weather radars to measure full vector wind fields^{2,42}; and the bistatic radar for weapons location.³⁵

Furthermore, major progress has been made in developing signal and data processing algorithms, including bistatic SAR autofocus and image formation and space-time adaptive processing for bistatic airborne MTI (see Section 23.5). However, two problems continue to plague bistatic and multistatic radars and have become the topics of this section: (1) beam scan-on-scan for bistatic radars and radar hitchhikers and (2) noncooperative RF environments for passive bistatic radars. These problems and their potential remedies are detailed next.

Beam Scan-on-Scan. When high-gain, narrow-beam scanning antennas are used by both transmitter and receiver in a bistatic surveillance radar, inefficient use is made of the radar energy because only the volume common to both beams can be observed by the receiver at any given time. Outside this common beam volume, targets are lost to the receiver. Figure 23.10 shows the geometry. This problem commonly arises when attempting to hitchhike off monostatic surveillance radars. Four remedies are available to mitigate the beam scan-on-scan problem: (1) step scanning, (2) flood-light beams, (3) multiple beams, and (4) time-multiplexed beams, which in the limit is called *pulse chasing*.

Step Scanning. For hitchhiking, the step scanning remedy consists of fixing the receive beam and waiting for the transmit beam to scan through the surveillance sector. The receive beam is then stepped one beamwidth for the next transmit beam scan and so on, until the receive beam has stepped across the full surveillance sector. For a dedicated transmitter, the process can be reversed: fix the transmit beam and scan the receive beam. This remedy increases the surveillance frame time by the number of required beam steps and is usually not acceptable for large area surveillance. It can be considered in an over-the-shoulder geometry or when the baseline is small. In these cases, transmit and receive beams become more closely aligned in a

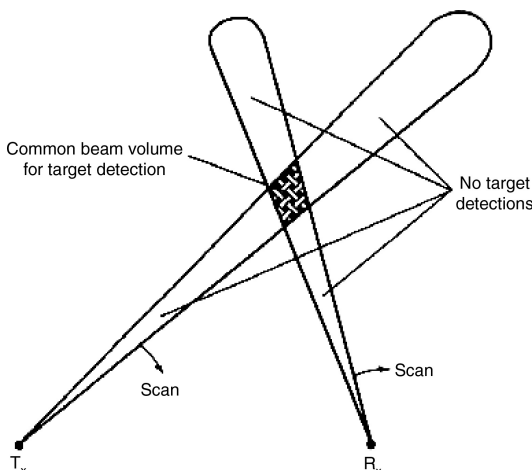


FIGURE 23.10 Beam scan-on-scan coverage problem shown in two dimensions in the bistatic plane² (*Courtesy SciTech*)

pseudo-monostatic geometry, which reduces the number of required beam steps. The *Bistatic Radar for Weapons Location* test program³⁵ is an example.

Floodlight Beams. A floodlight beam can be used with either transmitter or receiver. The floodlight transmitter remedy requires a dedicated transmit antenna that is designed to flood the surveillance sector continuously. The receiver then scans the sector with a high-gain antenna. This remedy restores the surveillance frame time lost by step scanning while simultaneously servicing multiple receivers. However, it incurs a detection range penalty by the reduced transmit antenna gain and also suffers increased sidelobe clutter levels. The floodlight receiver remedy can be used by a hitchhiker to flood a sector scanned by the transmit beam, again restoring the surveillance frame time. In addition to the range penalty, the receiver will also suffer increased clutter levels and angle measurement errors. Despite these limitations, the *Binet* floodlight receiver was found quite adequate for measuring three dimensional vector wind fields.^{2,42}

Multiple Beams. A bistatic receiver can use multiple simultaneous fixed receive beams to cover the surveillance sector, which again restores the surveillance frame time. If the gain of each receive antenna is made equal to the gain of the initial single receive antenna, range performance is also restored. However, this remedy increases the cost and complexity of the receiver since a special beamforming network is required, along with a receiver and signal processor (RSP) for each beam. The multi-beam receiver can be used with any type of transmitter, including a floodlight transmitter where the loss in range performance might be offset by an increase in dwell time on target, as detailed subsequently.

Time-multiplexing. If the transmitter's beam scanning schedule is known, the number of receive beams (and RSPs) can be reduced in some geometries by time-multiplexing them to cover only the currently illuminated surveillance sector.

For example, in an over-the-shoulder geometry, the receiver might use a set of beams to cover the north side of the baseline; then, as the transmit beam scans past the receiver, it switches the set to the south side, thus halving the total number required. The *Bistatic Alerting and Cueing* test program used time-multiplexed beams when hitchhiking off the AWACS transmitter for short-range air surveillance.^{46,47}

Pulse Chasing. If the transmitter's beam scanning and pulse transmission schedule are known, pulse chasing can be considered to reduce the multibeam cost penalty further.^{1,21,115–118} This was successfully demonstrated in the *Bistatic Radar for Weapons Location* test program.³⁵ The simplest pulse-chasing concept uses a single beam and RSP that rapidly scans the volume covered by the transmit beam, chasing the pulse as it propagates from the transmitter. The receive beam-scanning rate must be at the transmitter's pulse propagation rate, modified by the usual geometric conditions. This rate, $\dot{\theta}_R$, was initially identified by Jackson²¹ and subsequently verified by Moyer and Morgan¹¹⁹:

$$\dot{\theta}_R = c \tan(\beta/2)/R_R \quad (23.18)$$

For operation in the co-site region (see Table 23.2), $\dot{\theta}_R$ can vary from $1^\circ/\mu\text{s}$ near the baseline to $0.01^\circ/\mu\text{s}$ when $R_T + R_R > L$. Typical $\dot{\theta}_R$ contours are shown in Jackson.²¹ These rates and rate changes require an inertialess antenna, for example, a phased array with diode phase shifters. Normally, a phased array antenna used for surveillance is programmed to switch beams in increments of a beamwidth. Fractional shifts of a beamwidth can be achieved by changing the phase of a few (symmetric) pairs of phase shifters in the array. In this way, a pseudo-continuous beam scan can be generated with the required rates and rate changes.¹²⁰

Because of pulse propagation delays from the target to the receiver, the pointing angle of the receive beam θ_R must lag the actual pulse position. For an instantaneous pulse position that generates a bistatic angle $\beta/2$, $\theta_R = \theta_T - \beta$. In terms of the bistatic triangle, the required receive beam-pointing angle is²¹

$$\theta_R = \theta_T - 2 \tan^{-1} \left(\frac{L \cos \theta_T}{R_T + R_R - L \sin \theta_T} \right) \quad (23.19)$$

The minimum receive beamwidth $(\Delta\theta_R)_m$ required to capture all returns from a range cell intersecting the common beam area is approximated by²¹

$$(\Delta\theta_R)_m \approx (c \tau_u \tan(\beta/2) + \Delta\theta_T R_T)/R_R \quad (23.20)$$

where τ_u is the uncompressed pulse width and $\Delta\theta_T$ is the transmit beamwidth. The approximation assumes that respective rays from the transmit and receive beams are parallel. The approximation is reasonable when $(R_T + R_R) \gg L$ or when $L \gg c\tau_u$. Equation 23.20 shows that $(\Delta\theta_R)_m$ changes as the receive beam scans out the transmit beam. Phased array antennas operating with a digital beamformer^{59,60} can accommodate this change. Otherwise, use of a fixed beamwidth incurs a small beam mismatch loss. An example is given in Willis.¹

Even though one pulse must be chased at a time, a hitchhiker operating in the co-site region has time to capture all pulses from a monostatic radar that uses range-unambiguous PRFs. Furthermore, when operating in the transmit- or receive-centered ovals (refer to Table 23.2) a hitchhiker can operate with range-ambiguous PRFs, for example, when transmitted from an airborne radar. Examples are given in Willis.¹

Other implementations of pulse chasing are possible. In one concept, the fixed multibeam receive antenna is used and two RSPs are time-multiplexed across the multibeams. One RSP steps across the even-numbered beams, and the other RSP steps across the odd-numbered beams, so that returns in beam pairs are processed simultaneously: (1,2), (2,3), (3,4), etc. This *leapfrog* sequence is required to capture all returns in the common-beam area.

A second concept uses two beams and two RSPs step-scanning over the volume covered by the multibeam antenna. It uses an identical leapfrog sequence. Both concepts relax the fractional beam scan requirements by either sampling or stepping the beams in units of a beamwidth. Since they both process returns across two beamwidths before switching, the beam dwell time T_b is approximately $2(\Delta\theta_R)_m R_R/c$ and the stepping rate is T_b^{-1} . The approximation assumes negligible phase-shift delays and settling times.

Moving Target Indication (MTI) can be used with any of these pulse chasing implementations, as long as the receive beam precisely retraces its scan pattern on successive sweeps to capture the same clutter samples over the MTI processing time.

Combinations. Combinations of these remedies can be considered. For example, a fixed multibeam receive antenna can be used with a fixed floodlight transmit antenna. This configuration allows the receiver to integrate longer, subject to target/cell migration limits, which, in turn, can recover some of the lost range performance of the floodlight antenna. It also has the benefits of increasing data rates and simultaneously servicing multiple receivers. It incurs increased sidelobe clutter levels, as well as complexity and cost. Some passive bistatic radars operate in this configuration, where the floodlight transmitter is provided by a TV or FM broadcast station.^{49,50}

A single receive beam can be used with a transmit antenna that is adaptively tapered to flood only the angular region covered by the receive beam at a given look angle, with the tapering such that the signal-to-noise ratio at the receiver is held constant at all positions along the receive beam. This scheme is analogous to the monostatic air surveillance radar using a cosecant-squared antenna pattern, where the echo is independent of range for a constant altitude target.¹⁵ It has the potential of restoring much of the frame time and range performance, but incurs increased sidelobe clutter levels and increased transmitter cost and complexity. An example is given in Willis.¹

Noncooperative RF Environment. Most passive bistatic radar (PBR) concepts and developments exploit commercial broadcast transmitters as their source of radar illumination. FM and High Definition (HD) TV terrestrial broadcast transmitters are particularly attractive due to their high-power, noise-like waveforms, and relatively wide bandwidths.^{49–51} When these broadcast transmitters are appropriately sited and operating, they can support many types of surveillance, particularly air surveillance, which is often restricted for monostatic radars operating at VHF/UHF. The surveillance can be covert because even the transmitter is unaware it is being exploited and can be counter-stealth due to unavoidable aircraft resonances in the VHF/UHF region. Other attractive features are lower prime power requirements and lower costs for the PBR.²

While a PBR can exploit both cooperative and noncooperative broadcast transmitters, the PBR has no control over their transmission or waveform properties, specifically the transmission schedule, effective radiated power, spatial coverage, modulation type, modulation content, and resulting autocorrelation function, as outlined earlier. Furthermore, interference from the host emitter and other emitters, especially in urban and suburban areas, can significantly degrade PBR performance. This section summarizes the problems and remedies encountered by a PBR exploiting these broadcast transmitters.

Waveforms. The effective radiated power (ERP) of broadcast transmitters can vary from a maximum of ~1 MW for TV transmitters to a minimum of ~10 W for cell-phone tower transmitters. The former can yield equivalent monostatic detection ranges of air targets of 100–150 km; the latter, 1–5 km, which is of the order of the cell-phone waveform resolution, typically 2 km.² Consequently when these low-powered transmitters are evaluated for short-range ground or air target location,¹²¹ only doppler (and coarse DOA) data are available, which severely restricts location capability, as outlined in Section 23.6. Thus, the low ERP of these transmitters constrained by the available bandwidth conspire to significantly reduce their utility for PBR surveillance.

The type of modulation used by a broadcast transmitter is particularly important. For example, the 1985 Crystal Palace TV transmitter trials in London¹²² attempted range measurements with analog TV waveforms but found that they generated high range sidelobes (~5 dB), range ambiguities every 9.6 km, and modest range resolution (~4 km), and concluded that such waveforms were more suitable for doppler measurements. This finding established the precedence for subsequent PBR developments: doppler exploitation of stable, narrow-band carrier lines in TV transmissions and range/doppler exploitation of the wider band, noise-like spectrum of FM transmissions.

The modulation content of many broadcast transmitters changes as a function of time, thereby complicating matched filtering by the PBR's receiver. Specifically, the receiver must sample and store a segment of the direct path waveform and then cross-correlate it with the returned echo, all in real time. Since cross-correlation must be performed over the range of expected target echo time delays and/or doppler shifts, correlation receiver complexity is increased with respect to a matched-filter receiver typically used by monostatic radar.¹²³ Such cross-correlation is now feasible to implement, but complicates an otherwise well-developed operation in the stable, more predictable monostatic world.

A related modulation content problem is *dead air*, where no information is broadcast; thus, the broadcast transmitter modulation goes to zero and range measurement errors increase without limit. This condition can occur when broadcasting a talk show or classical music, but occurs less often with popular or rock music.¹²⁴ The frequency of this type of outage is not insignificant, occurring roughly once per second for talk broadcasts.¹²⁵ Consequently, once a track has been established a nonlinear tracking filter may be needed to edit out large error spikes (see Chapter 6 of Willis and Griffiths.²)

Radio Frequency Interference. Passive bistatic radar performance is subject to degradation by radio frequency interference (RFI) from both the exploited broadcast transmitter and other emitters in spatial or frequency proximity. These emitters can include broadcast, communications, and navigation transmitters, as well as power tools, fluorescent lights, cooling fans, and (old) automobile ignitions, which typically generate impulsive noise.* RFI can arrive via a direct path or multipath and includes scattering from terrain or sea surfaces, also called clutter. However, the signal from an exploited transmitter arriving over the direct transmitter-to-receiver path, called the *direct-path*, is nearly always the dominant RFI source. Multipath signals from that transmitter are less severe but can also contribute to RFI.

RFI over the direct-path from the exploited transmitter, also called *direct-path breakthrough*, is common to all but the simplest, low-power CW radar. It becomes

* Sky noise consisting of sun, galactic, and atmospheric noise is another source of RFI, which can increase the receiver's noise temperature by a factor of 2–4 at frequencies below ~400 MHz.³⁰ However, this increase is usually orders of magnitude smaller than RFI from other sources and can be ignored.

particularly severe when the receiver is located in direct LOS of the transmitter, which must occur when surveillance of low-altitude air targets is required (Eqs. 23.5–23.8). If this direct path signal is not attenuated, the received signal becomes masked in range and often masked in doppler by sidelobes of the correlated direct path signal.

Direct-path breakthrough effects are similar to those of a spot noise jammer and can be characterized by an increase in the system noise temperature, $T_s = F_n T_o$, where F_n is the receiver noise figure and $T_o = 290$ K. Specifically, the amount of increase in T_s , and hence the amount of attenuation C_{dp} required to reduce the direct path signal to the level of T_s , is

$$C_{dp} = P_T G_T (G_R)_T \lambda^2 / (4\pi)^2 B L^2 (kT_s) \quad (23.21)$$

where P_T , G_T , λ , and k are defined with Eq. 23.2; $(G_R)_T$ is the receiving antenna power gain in the direction of the transmitter; B is the input RF bandwidth; and L is the baseline range.

For example, if the PBR exploits a typical FM broadcast transmitter located at a 50 km LOS from the receiver, $P_T G_T = 250$ kW, $\lambda = 3$ m, $B = 50$ kHz, and $L = 50$ km. Assuming a fixed receiving antenna beam tailored in elevation and covering a wide azimuth sector, which includes the transmitter site, $(G_R)_T$ might be 8 dBi. Also, assuming the ambient RFI environment described below, the noise spectral density $kT_s = -179$ dBW/Hz; thus, $C_{dp} = 88$ dB.

Combinations of earth masking, antenna shielding, spatial cancellation, and spectral cancellation can be used to achieve the required direct-path attenuation. A brute-force remedy is to physically block the transmit signal from the receiver with a shroud or structure, or if coverage allows, over-the-horizon separation. While many orders of magnitude attenuation are possible with these masking and shielding techniques, additional reduction is nearly always necessary. Howland reported a two-stage, spatial noise canceller with an adaptive M-stage lattice predictor ($M = 50$) as the first stage and an adaptive tapped delay line as the second stage, which achieved ~75 dB cancellation of the narrow-band stationary direct path signal.^{113,114} This cancellation combined with masking achieved >90 dB attenuation, which satisfies the C_{dp} requirement in the above example. Howland also observed that receiver dynamic range ultimately limits the available cancellation, which, in turn, is set by the receiver's analog-to-digital converter.

Nearby emitters can significantly raise the system noise level, simply through spectral spillover from adjacent or nearby bands. In the U.S. the FCC mandates a gaussian spectral roll-off for many broadcast transmitters, which is sufficient to prevent interference in one-way home receivers from adjacent transmissions. However, it is not sufficient for two-way radar receivers, which necessarily must work much farther into the receiver noise.¹²⁶

The severity of this problem was quantified by in situ measurements of several VHF and UHF bands in a dense urban environment.¹²⁷ Ambient VHF noise levels were found to be typically 45 dB greater than thermal noise and direct path illuminator signals some 45 dB greater still. Even with robust cancellation techniques, the residue of this un suppressed RFI will increase the PBR's system noise figure by many tens of decibels: a 25 dB noise figure at VHF in urban and semi-rural areas is not uncommon.¹²⁶ This value translates into a noise spectral density of -179 dBW/Hz. Similar measurements have been made at UHF, with 20–25 dB noise figures being obtained using spectral cancellation by a least-squares channel estimator.⁵¹ These noise figures are significantly higher than those obtained in the U.S. radar-designated VHF/UHF channels and are a penalty for exploiting broadcast transmitters of opportunity.

REFERENCES

1. N. J. Willis, *Bistatic Radar*, 2nd Ed., Silver Spring, MD: Technology Service Corp., 1995. Corrected and republished by Raleigh, NC: SciTech Publishing, Inc., 2005.
2. N. J. Willis and H. D. Griffiths, (eds.), *Advances in Bistatic Radar*, Raleigh NC: SciTech Publishing Inc., 2007.
3. R. C. Heimiller, J. E. Belyea, and P. G. Tomlinson, "Distributed array radar," *IEEE Trans.*, vol. AES-19, pp. 831–839, 1983.
4. B. D. Steinberg, *Principles of Aperture and Array System Design—Including Random and Adaptive Arrays*, New York: John Wiley & Sons, 1976.
5. B. D. Steinberg and E. Yadin, "Distributed airborne array concepts," *IEEE Trans.*, vol. AES-18, pp. 219–226, 1982.
6. B. D. Steinberg, "High angular microwave resolution from distorted arrays," *Proc. Int. Comput. Conf.*, vol. 23, 1980.
7. T. C. Cheston and J. Frank, "Phased array antennas," Chapter 7 in *Radar Handbook*, M. I. Skolnik, (ed.), 2nd Ed., New York: McGraw-Hill, 1990.
8. L. E. Mertens and R. H. Tabeling, "Tracking instrumentation and accuracy on the Eastern Test Range," *IEEE Trans.*, vol. SET-11, pp. 14–23, March 1965.
9. J. J. Scavullo and F. J. Paul, *Aerospace Ranges: Instrumentation*, Princeton, NJ: D. Van Nostrand Company, 1965.
10. B. D. Steinberg, et al., "First experimental results for the Valley Forge radio camera program," *Proc. IEEE*, vol. 67, pp. 1370–1371, September 1979.
11. B. D. Steinberg, "Radar imaging from a distributed array: The radio camera algorithm and experiments," *IEEE Trans.*, vol. AP-29, pp. 740–748, September 1981.
12. "Handbook for NAVSPASUR System Orientation," vol. 1, Naval Space Surveillance System, Dahlgren, VA, July 1, 1976.
13. M. I. Skolnik, "An analysis of bistatic radar," *IRE Trans.*, vol. ANE-8, pp. 19–27, March 1961.
14. J. M. Caspers, "Bistatic and multistatic radar," Chapter 36 in *Radar Handbook*, M. I. Skolnik, (ed.), New York: McGraw-Hill Book Company, 1970.
15. M. I. Skolnik, *Introduction to Radar Systems*, New York: McGraw-Hill Book Company, 1980.
16. N. J. Willis, "Bistatic radar," Chapter 25, in *Radar Handbook*, M. I. Skolnik (ed.), 2nd Ed., New York: McGraw-Hill, 1990.
17. E. F. Ewing, "The applicability of bistatic radar to short range surveillance," in *IEE Conf. Radar 77, Publ. 155*, London, 1977, pp. 53–58.
18. E. F. Ewing and L. W. Dicken, "Some Applications of Bistatic and Multi-Bistatic Radars," in *Int. Radar Conf.*, Paris, 1978, pp. 222–231.
19. A. Farina and E. Hanle, "Position accuracy in netted monostatic and bistatic radar," *IEEE Trans.*, vol. AES-19, pp. 513–520, July 1983.
20. E. Hanle, "Survey of bistatic and multistatic radar," *Proc. IEE*, vol. 133, pt. F, pp. 587–595, December 1986.
21. M. C. Jackson, "The geometry of bistatic radar systems," *IEE Proc.*, vol. 133, pt. F, pp. 604–612, December 1986.
22. D. E. N. Davies, "Use of bistatic radar techniques to improve resolution in the vertical plane," *IEE Electron. Lett.*, vol. 4, pp. 170–171, May 3, 1968.
23. J. R. Forrest and J. G. Schoenenberger, "Totally independent bistatic radar receiver with real-time microprocessor scan correction," *IEEE Int. Radar Conf.*, 1980, pp. 380–386.
24. J. G. Schoenenberger and J. R. Forrest, "Principles of independent receivers for use with co-operative radar transmitters," *Radio Electron. Eng.*, vol. 52, pp. 93–101, February 1982.
25. E. G. McCall, "Bistatic clutter in a moving receiver system," *RCA Rev.*, pp. 518–540, September 1969.

26. H. A. Crowder, "Ground clutter isodops for coherent bistatic radar," *IRE Nat. Conv. Rec.*, pt. 5, New York, 1959, pp. 88–94.
27. L. J. Cantafio (ed.), *Space-Based Radar Handbook*, Chapter 5, Norwood, MA: Artech House, 1989.
28. A. Farina and F. A. Studer, *Radar Data Processing*, Vol. 2, *Advanced Topics and Applications*, UK: Research Studies Press Ltd., 1986.
29. I. Stein, "Bistatic radar applications in passive systems," *Journal of Electronic Defense*, 13(3), pp. 55–61, March 1990.
30. D. K. Barton, *Modern Radar System Analysis*, Norwood, MA: Artech House, 1988.
31. D. K. Barton, private communication, June 2006.
32. R. L. Easton and J. J. Fleming, "The Navy space surveillance system," *Proc. IRE*, vol. 48, pp. 663–669, 1960.
33. R. J. Lefevre, "Bistatic radar: New application for an old technique," *WESCON Conf. Rec.*, San Francisco, 1979, pp. 1–20.
34. F. L. Fleming and N. J. Willis, "Sanctuary radar," *Proc. Mil. Microwaves Conf.*, London, October 22–24, 1980, pp. 103–108.
35. L. Bovino, "Bistatic radar for weapons location," U.S. Army Communications Electronics Command, Fort Monmouth, NJ, 1994.
36. Russia's Arms Catalog, vol. 5, Air Defense, Moscow: Military Parade Ltd., 1997.
37. "Barrier." Bistatistical low flying target detection system, Nizhny Novgorod Scientific-Research Radiotechnical Institute, Moscow, 2000.
38. A. G. Blyakhman et al., "Forward scattering radar moving object coordinate measurement," *IEEE International Radar Conference*, 2000.
39. A. Thomson, *A GRAVES Sourcebook*, version of 2006-10-27, thomsona@flash.net.
40. J. E. Salah and J. E. Morriello, "Development of a multistatic measurement system," in *IEEE International Radar Conference*, 1980, pp. 88–93.
41. "Multistatic mode raises radar accuracy," *Aviation Week and Space Technology*, pp. 62–69, July 14, 1980.
42. J. Wurman, S. Heckman, and D. Boccippio, "A bistatic multiple-doppler radar network," *Journal of Applied Meterology*, vol. 32, pp. 1802–1814, December 1993.
43. J. Wurman, M. Randall, C. L. Brush, E. Loew, and C. L. Holloway, "Design of a bistatic dual-doppler radar for retrieving vector winds using one transmitter and a remote low-gain passive receiver," invited paper, *Proc. of the IEEE*, vol. 82, no. 12, December 1994, pp. 1861–1872.
44. F. Johnson, *Synthetic Aperture Radar (SAR) Heritage: An Air Force Perspective*, Ohio: Air Force Avionics Laboratory, Wright Patterson AFB, June 2003.
45. D. C. Lorti and M. Balser, "Simulated performance of a tactical bistatic radar system," *IEEE EASCON 77 Rec. Publ. 77 CH1255-9*, Arlington, VA, 1977, pp. 4-4A–4-40.
46. "Bistatic Radars Hold Promise for Future System," *Microwave Systems News*, pp. 119–136, October 1984.
47. E. C. Thompson, "Bistatic radar noncooperative illuminator synchronization techniques," in *Proc. of the 1989 IEEE National Radar Conference*, Dallas, TX, March 29–30, 1989.
48. J. D. Sahr, "Remote sensing with passive radar at the University of Washington," *IEEE Geoscience and Remote Sensing Society Newsletter*, pp. 16–21, December 2005.
49. "Passive system hints at stealth detection silent sentry—A new type of radar," *Aviation Week and Space Technology*, November 30, 1998, pp. 70–71.
50. J. Baniak, G. Baker, A. M. Cunningham, and L. Martin, "Silent Sentry™ Passive Surveillance," *Aviation Week and Space Technology*, June 7, 1999.
51. A. Andrews, "HDTV-based passive radar," presented at AOC 4th Multinational PCR Conference, Syracuse, NY, October 6, 2005.
52. R. A. Simpson, "Spacecraft studies of planetary surfaces using bistatic radar," *IEEE Trans. Geoscience and Remote Sensing*, vol. 31 no. 2, March 1993.

53. D. Prichard, *The Radar War: The German Achievement, 1904–1945*, Cambridge, UK: Patrick Stephens Ltd., 1989.
54. A. Price, *Instruments of Darkness: The History of Electronic Warfare*, New York: Charles Scribner's Sons, 1978.
55. P. J. Klass, "Navy improves accuracy, detection range," *Aviation Week and Space Technology*, pp. 56–61, August 16, 1965.
56. *Technology in the National Interest*, Lexington, MA: MIT Lincoln Laboratory, 1995.
57. A. Bernard, private communication, MIT Lincoln Laboratory, July 24, 2006.
58. S. Satoh and J. Wurman, "Accuracy of wind fields observed by a bistatic doppler radar network," *Journal Ocean. Atmos. Tech.* vol. 20, pp. 1077–1091, 2003.
59. A. E. Ruvin and L. Weinberg, "Digital multiple beamforming techniques for radars," in *IEEE Eascon '78 Rec.*, pp. 152–163.
60. E. E. Swartzlander and J. M. McKay, "A digital beamforming processor," *Real Time Signal Processing III, SPIE Proc.*, vol. 241, pp. 232–237, 1980.
61. A. Farina, "Tracking function in bistatic and multistatic radar systems," *Proc. IEE*, vol. 133, pt. F, pp. 630–637, December 1986.
62. R. B. Patton, Jr., "Orbit determination from single pass doppler observations," *IRE Transactions on Military Electronics*, pp. 336–344, April–July, 1960.
63. A. Farina, "Tracking function in bistatic and multistatic radar systems," *IEE Proc.*, 133(7), pt. F, pp. 630–637, December 1986.
64. M. I. Skolnik, *Introduction to Radar Systems*, New York: McGraw Hill Book Co., 1962.
65. D. K. Barton, *Radar System Analysis*, Dedham, MA: Artech House, Inc., 1976.
66. K. M. Siegel, et al., "Bistatic radar cross sections of surfaces of revolution," *J. Appl. Phys.*, vol. 26, pp. 297–305, March 1955.
67. K. M. Siegel, "Bistatic radars and forward scattering," in *Proc. Nat. Conf. Aeronaut. Electron.*, May 12–14, 1958, pp. 286–290.
68. F. V. Schultz et al., "Measurement of the radar cross-section of a man," *Proc. IRE*, vol. 46, pp. 476–481, February 1958.
69. J. W. Crispin, Jr. et al., "A theoretical method for the calculation of radar cross section of aircraft and missiles," University of Michigan, Radiation Lab. Rept. 2591-1-H, July 1959.
70. R. E. Hiatt et al., "Forward scattering by coated objects illuminated by short wavelength radar," *Proc. IRE*, vol. 48, pp. 1630–1635, September 1960.
71. R. J. Garbcz and D. L. Moffett, "An experimental study of bistatic scattering from some small, absorber-coated, metal shapes," *Proc. IRE*, vol. 49, pp. 1184–1192, July 1961.
72. M. G. Andreasen, "Scattering from bodies of revolution," *IEEE Trans.*, vol. AP-13, pp. 303–310, March 1965.
73. C. R. Mullin et al., "A numerical technique for the determination of the scattering cross sections of infinite cylinders of arbitrary geometric cross section," *IEEE Trans.*, vol. AP-13, pp. 141–149, January 1965.
74. R. E. Kell, "On the derivation of bistatic RCS from monostatic measurements," *Proc. IEEE*, vol. 53, pp. 983–988, August 1965.
75. W. I. Kock, "Related experiments with sound waves and electromagnetic waves," *Proc. IRE*, vol. 47, pp. 1200–1201, July 1959.
76. K. M. Siegel et al., "RCS calculation of simple shapes—bistatic," Chapter 5 in *Methods of Radar Cross-Section Analysis*, New York: Academic Press, 1968.
77. H. Weil et al., "Scattering of electromagnetic waves by spheres," University of Michigan, Radiat. Lab. Stud. Radar Cross Sections X, Rept. 2255-20-T, contract AF 30(602)-1070, July 1956.
78. R. W. P. King and T. T. Wu, *The Scattering and Diffraction of Waves*, Cambridge, MA: Harvard Universities Press, 1959.
79. R. F. Goodrich et al., "Diffraction and scattering by regular bodies—I: The sphere," University of Michigan, Dept. Electr. Eng. Rept. 3648-1-T, 1961.

80. M. Matsuo et al., "Bistatic radar cross section measurements by pendulum method," *IEEE Trans.*, vol. AP-18, pp. 83–88, January 1970.
81. G. W. Ewell and S. P. Zehner, "Bistatic radar cross section of ship targets," *IEEE J. Ocean. Eng.*, vol. OE-5, pp. 211–215, October 1980.
82. "Radar cross-section measurements," General Motors Corporation, Delco Electron. Div. Rept. R81-152, Santa Barbara, CA, 1981.
83. C. G. Bachman, *Radar Targets*, Lexington, MA: Lexington Books, 1982, p. 29.
84. F. C. Paddison et al., "Large bistatic angle radar cross section of a right circular cylinder," *Electromagnetics*, vol. 5, pp. 63–77, 1985.
85. J. I. Glaser, "Bistatic RCS of complex objects near forward scatter," *IEEE Trans.*, vol. AES-21, pp. 70–78, January 1985.
86. C.-C. Cha et al., "An RCS analysis of generic airborne vehicles' dependence on frequency and bistatic angle," in *IEEE Nat. Radar Conf.*, Ann Arbor, MI, April 20, 1988, pp. 214–219.
87. W. A. Pierson et al., "The effect of coupling on monostatic-bistatic equivalence," *Proc. IEEE*, pp. 84–86, January 1971.
88. "Bistatic radars hold promise for future systems," *Microwave Syst. News*, pp. 119–136, October 1984.
89. M. M. Weiner, "Multistatic radar phenomenology terrain & sea scatter," RADC-TR-81-75, vol. 1, May 1981, now unlimited distribution.
90. S. T. Cost, "Measurements of the bistatic echo area of terrain at X-band," The Ohio State University, Antenna Laboratory, Report No. 1822-2, May 1965.
91. W. H. Peake and S.T. Cost, "The bistatic echo area of terrain at 10 GHz," in *IEEE WESCON 1968*, Session 22/2, pp. 1–10.
92. V. W. Pidgeon, "Bistatic cross section of the sea," *IEEE Trans. AP-14(3)*, pp. 405–406, May 1966.
93. V. W. Pidgeon, "Bistatic cross section of the sea for Beauford 5 sea," in *Science and Technology*, vol. 17 "Use of space systems for planetary geology and geophysics," San Diego: American Astronautical Society, 1968, pp. 447–448.
94. A. R. Domville, "The bistatic reflection from land and sea of X-band radio waves, Part I," GEC (Electronics) Ltd., Stanmore, England, Memorandum SLM1802, July 1967.
95. A. R. Domville, "The bistatic reflection from land and sea of X-band radio waves, Part II," GEC (Electronics) Ltd., Stanmore, England, Memorandum SLM2116, July 1968.
96. A. R. Domville, "The bistatic reflection from land and sea of X-band radio waves, Part II-supplement," GEC (Electronics) Ltd., Stanmore, England, Memorandum SLM2116 (Supplement), July 1969.
97. R. W. Larsen and R. C. Heimiller, "Bistatic clutter data measurement program," Environmental Research Institute of Michigan, RADC-TR-77-389, November 1977, AD-A049037.
98. R. W. Larsen, A. L. Maffett, R. C. Heimiller, A. F. Fromm, E. L. Johansen, R. F. Rawson, and F. L. Smith, "Bistatic clutter measurements," *IEEE Trans. AP-26(6)*, pp. 801–804, November 1978.
99. R. W. Larsen, A. Maffett, F. Smith, R.C. Heimiller, and A. Fromm, "Measurements of bistatic clutter cross section," Environmental Research Institute of Michigan, Final Technical Report RADC-TR-79-15, May 1979, AD-A071193.
100. P. E. Cornwell and J. Lancaster, "Low-altitude tracking over rough surfaces II: Experimental and model comparisons," in *IEEE EASCON-79 Record*, October 1979, pp. 235–248.
101. G. W. Ewell and S. P. Zehner, "Bistatic sea clutter return near grazing incidence," in *IEE Int. Conf. Radar 82*, Publication No. 216, London, October 1982, pp. 188–192.
102. G. W. Ewell, "Techniques of radar reflectivity measurement," Chapter 7 in *Bistatic Radar Cross-Section Measurements*, 2nd Ed., N. C. Currie (ed.), Norwood, MA: Artech House, 1984.
103. F. T. Ulaby, T. E. Van Deventer, J. R. East, T. F. Haddock, and M. E. Coluzzi, "Millimeter-wave bistatic scattering from ground and vegetation targets," *IEEE Trans. GRS-26(3)*, pp. 229–243, May 1988.

104. T. P. Kochanski, M. J. Vanderhill, J.V. Zolotarevsky, and T. Fariss, "Low illumination angle bistatic sea clutter measurements at X-band," in *IEEE Int. Conf. Oceans-92: Mastering the Oceans Through Technology, Proc.*, vol. 1, October 26–29, 1992, pp. 518–523.
105. D. J. McLaughlin, E. Boltniew, Y. Wu, and R. S. Raghavan, "Low grazing angle bistatic NCRS of forested clutter," *Electronics Letters*-30(18), pp. 1532–1533, September 1, 1994.
106. D. J. McLaughlin, E. Boltniew, R. S. Raghavan, and M. J. Sowa, "Cross-polarized bistatic clutter measurements," *Electronics Letters*-31(6), pp. 490–491, March 16, 1995.
107. D. J. McLaughlin, Y. Wu, W. G. Stevens, X. Zhang, M. J. Sowa, and B. Weijers, "Fully polarimetric bistatic radar scattering behavior of forested hills," *IEEE Trans. AP-50(2)*, pp. 101–110, February 2002.
108. R. E. Vander Schur and P. G. Tomlinson, "Bistatic clutter analysis," Decision-Sciences Applications, Inc., RADC-TR-79-70, April 1979.
109. G. O. Sauermann and P. C. Waterman, "Scattering modeling: Investigation of scattering by rough surfaces," MITRE Corporation, Rept. MTR-2762, AFAL-TR-73-334, January 1974.
110. J. G. Zornig et al., "Bistatic surface scattering strength at short wavelengths," Yale University, Dept. Eng. Appl. Sci. Rept. CS-9, AD-A041316, June 1977.
111. E. N. Bramley and S. M. Cherry, "Investigation of microwave scattering by tall buildings," *Proc. IEE*, vol. 120, pp. 833–842, August 1973.
112. A. E. Brindly et al., "A Joint Army/Air Force investigation of reflection coefficient at C and K_u bands for vertical, horizontal and circular system polarizations," IIT Research Institute, Final Rept., TR-76-67, AD-A031403, Chicago, IL, July 1976.
113. P. E. Howland, D. Maksymiuk, and G. Reitsma, "FM radio based bistatic radar," *IEE Proc.-Radar Sonar Navig.*, vol. 152, no. 3, pp. 107–115, June 2005.
114. P. E. Howland, "FM-radio based bistatic radar," presented at AOC 4th Multinational PCR Conference, Syracuse, NY, October 6, 2005.
115. T. A. Soame and D. M. Gould, "Description of an experimental bistatic radar system," in *IEE Int. Radar Conf. Publ.* 281, 1987, pp. 12–16.
116. E. Hanle, "Pulse chasing with bistatic radar-combined space-time filtering," in *Signal Processing II: Theories and Applications*, H. W. Schussler (ed.), North Holland: Elsevier Science Publishers B. V., pp. 665–668.
117. J. G. Schoenenberger and J. R. Forrest, "Principles of independent receivers for use with co-operative radar transmitters," *Radio Electron. Eng.*, vol. 52, pp. 93–101, February 1982.
118. N. Freedman, "Bistatic radar system configuration and evaluation," Raytheon Company, Independ. Dev. Proj. 76D-220, *Final Rept. ER76-4414*, December 30, 1976.
119. L. R. Moyer, "Comments on 'Receiver antenna scan rate requirements needed to implement pulse chasing in a bistatic radar receiver,'" *IEEE Trans. on Aerospace and Electronic Systems*, vol. 38, no. 1, p. 300, January 2002, correspondence.
120. J. Frank and J. Ruze, "Beam steering increments for a phased array," *IEEE Trans.*, vol. AP-15, pp. 820–821, November 1967.
121. D. K. P. Tan, H. Sun, Y. Lu, M. Lesturgie, and H. L. Chan, "Passive radar using global system for mobile communication signal: Theory, implementation and measurements," *IEE Proc.-Radar Sonar Navig.*, vol. 152, no. 3, June 2005.
122. H. D. Griffiths and N. R. W. Long, "Television-based bistatic radar," *IEE Proc.*, 133(7), Pt. F, pp. 649–657, December 1986.
123. M. I. Skolnik, *Introduction to Radar Systems*, 3rd Ed., New York: McGraw-Hill, 2001.
124. H. D. Griffiths et al., "Measurement and analysis of ambiguity functions of off-air signals for passive coherent location," *Electronics Letters*, vol. 39, no. 13, June 26, 2003.
125. M. A. Ringer and G. J. Glazer, "Waveform analysis of transmissions of opportunity for passive radar," in *Fifth International Symposium on Signal Processing and its Applications*, Brisbane, Australia, August 1999, pp. 511–514.
126. Richard Lodwig, private communication, Lockheed Martin Mission Systems, 2003.
127. H. D. Griffiths and C. J. Baker, "Passive coherent location radar systems. Part 1: Performance prediction," *IEE Proc.-Radar Sonar Navig.*, vol. 152, no. 3, pp. 153–159, June 2005.